Anatomically-Based Laminated Models of Within-Area Integration in the Neocortex

Adrian Robert and Martin I. Sereno*
Cognitive Science Department, University of California at San Diego

SHORT TITLE: Anatomically-Based Laminated Models of Neocortex

Key words: layer, feedforward, feedback, neural model, propagation, neuroinformatics

* Corresponding author:

Martin I. Sereno
Department of Cognitive Science, 0515
University of California, San Diego
9500 Gilman Drive
La Jolla, CA 92093-0515
ph: 619-534-7449
fx: 619-534-1128
em: sereno@cogsci.ucsd.edu

Abstract

To lay groundwork for better testing theories of cortical function that may depend on interactions between multiple cortical layers, we constructed conductance-based spiking models of cortical circuitry with realistically differentiated cell types and lamination. Complexity, quantity, and inconsistency in anatomical data describing the circuitry were eliminated through application of constraint satisfaction and quantitative averaging techniques, which constitute a major contribution of this paper. In simulations, three dynamical regimes observed in slices were also observed in the model: transient response, wave propagation, and explosion. We found that, first, a 'tiered' lateral axonal arborization structure (several classes of arborization width) is in fact required to accurately model the lateral spread of stimulation-evoked activity demonstrated in electrophysiological and optical recording experiments. By excluding medium and longer range projections, activity propagation becomes slower but more robust than is actually observed. The longer connections thus may be sufficiently strong to affect computational processes such as Hebbian learning, in which the scale of lateral interactions is known to be important. Second, the model showed partial independence of activity in superficial and deep cortical layers, which depends on the laminar restriction of pyramidal axonal arbors found in many areas and many species. This partial uncoupling between laminae has also been seen experimentally. Thus, an area is likely to perform two distinct horizontal integrations of information at one x-y point in its superficial and deep layers.

Computational and simulation models of local neocortical networks are generally greatly simplified from the biological reality in several ways. At the individual unit level, compartmental cell models representing detailed electrochemical properties of the dendrites are typically eschewed in favor of single-compartment or "integrate-and-fire" neurons with just a few variables. This not only simplifies the tasks of simulation and/or analysis, but it makes the phenomenological behavior of the model easier to understand and use to derive insight into the functioning of the original system. At the circuit level, the architectural details are invariably boiled down to a largely schematic version of the original for similar reasons. The numbers of cell classes and the populations of each class are reduced, and connectivity matrices are correspondingly simplified. For both cell and circuitry, it is hoped that such simplifications do not fundamentally alter the functioning of the system respecting the phenomena being studied.

In the case of cell models, however, there is a large body of analytical work devoted to ensuring that this is so, and the parameters in the simplified models result from quantitative mathematical reduction (through processes such as integration of parameters over spatial and/or temporal domains) from experimentally-measured values in real cells (Bernander et al., 1994; Bush & Sejnowski, 1993; Lytton & Sejnowski, 1991; Segev et al., 1986). At the circuitry level, on the other hand, such rigorous standards have not been applied in neocortical models, for two major reasons. First, the anatomical data on cortical circuits is complex (in terms the number of cell classes, disagreement over their boundaries, the degree of specificity in connections, and so on) and often qualitatively reported (in the form of drawings, verbal descriptions, or numbers that are only indirectly related to quantities of interest). Second, even where the data is available in a tractable form, the appropriate mathematical reduction techniques are not always as obvious or as easily applied as in the single-cell case. With a single cell, clear criteria for fidelity in model behavior exist in terms of preservation of the response properties of the cell to various simple forms of stimulation, such as direct current injection or simulated synaptic input (Bush & Sejnowski, 1993). Such properties are easily measured experimentally by recording from a cell while stimulating it electrically or pharmacologically. However at the circuit level, not only do the types of possible and reasonable stimuli for gauging behavior occupy a much larger space, but both stimulation and measurement of the responses are more complex and face greater technical obstacles than is the case for single cells.

In the present work, we develop neocortical cell population and connectivity specifications by applying quantitative reduction techniques such as weighted averaging to anatomical data that has been augmented by constraint satisfaction. We then evaluate the functional fidelity of models constructed using our specifications by comparing their behavior under simulation to a set of slice physiology experiments chosen for their suitability for assessment of basic circuit transmission properties. The primary results we present here are, first, the techniques themselves for constructing the simplified models, showing how the available anatomical data may be sufficient for quantitative use if analytical tools are applied, and second, two insights derived from the model simulations into the relationship between neocortical anatomy and function that bear on present hypotheses regarding computational behavior. We preview each result in turn.

The anatomical data we use to derive a cortical circuit specification consists of information on the relative preponderances of various cell types, the proportions of other types they connect with, and how many synapses they form onto different dendritic portions – data which is mutually constraining by nature. If it

is known, for example, that cell type X sends 70% of its output of M synapses to spiny dendrites (possessed primarily by pyramidal cells) in layer IV, and that layer IV pyramidals receive N inputs of this type, then a direct quantitative relationship between the numbers of cell type X and of layer IV pyramidal cells in a section of neocortical tissue is established. If one of these numbers is known, perhaps through a similar relationship with some other cell type, the other one can be inferred. Many other such constraints can be found. To carry out a complete analysis, we collected data from the literature on a number of different areas and species, preferring data from rat primary sensory cortex where there were variations. Because in the classification we used (Jones & Peters, 1984) there are around dozen cell types in each layer connecting to around 10 other populations on average, it was impractical to work out all such relationships by hand. Instead we employed an iterative computational relaxation process to fill in the missing numbers.

The resulting estimates for cell class distribution and connectivity were combined with anatomical observations on the spatial arborization of dendrites and axons to determine a complex neocortical network architecture specification consisting of 51 distinct cell populations across 6 layers. Rather than instantiate a model from this directly, we reduced the number of layers and populations through weighted averaging. The resulting 3-layer, 13-population model was intended as a model of minimal complexity still preserving the basic vertical structure of neocortical circuitry. To assess the preservation of functional properties and their dependence on certain anatomical parameters, we simulated this model using single compartment, conductance-based model cells and compared it to neocortical slice physiology experiments (Chagnac-Amitai & Connors, 1989a,b; Langdon & Sur, 1990) measuring horizontal and vertical spread of activity following stimulation at a single point.

A further-reduced, 1-layer model with just two cell populations (excitatory and inhibitory) was constructed through additional weighted averaging. It was simulated and compared with the same experiments to study dependence of horizontal activity propagation on the lateral characteristics of axonal and dendritic arbors as well as the relative contribution of vertical structure. The model is also comparable to a number of existing 1-layer neocortical models studying both dynamics (Erwin et al., 1995; Wilson & Cowan, 1973) and connection development (Miller et al., 1989; Miller, 1994), allowing us to assess the functional differences introduced in our model by the quantitatively-reduced architecture.

We show in the Results that both the 3- and 1-layer versions of the cortical network capture several quantitative aspects of the experimental results without the use of any parameter fitting beyond the setting of the overall relative strengths of excitation and inhibition to obtain an appropriate dynamical regime. This suggested that our quantitative reduction in architectural detail left important functional properties intact. We also derived two novel insights into local neocortical integration through comparisons of the reduced anatomical data, the model behavior, and the physiological results.

The first was related to the fact that the simulations of the 3-layer model evidenced a surprising degree of independence between supra- and infragranular activity – e.g., infragranular cells could fire strongly over an extended period of time while supragranular cells remained silent. Although this runs contrary to the intuitive view of the neocortex as strongly vertically integrated, our quantitative analysis of the anatomical data showed that in fact connectivity is significantly weaker between supergranular and infragranular layers than within them. We also found corroboration of this result in previously-published physiological

experiments.

The second insight relates to the distribution of lateral connections made by pyramidal cells. By summing axonal arborization densities, we found that the collective influence a horizontally localized population of pyramidal cells has on the surrounding cells falls off discontinuously. In simulations, this resulted in higher propagation speeds and narrower wavelengths than seen when a smooth fall-off similar to that in many previous models was employed. Experimental results using simple forms of stimulation clearly agreed with the discontinous-falloff version, suggesting that this property is likely to have an effect on computational properties in more realistic situations.

These insights are only examples of how the techniques of anatomical compilation and quantitative reduction may aid modeling-based efforts at understanding cortical function. Similar techniques have been applied with success at the single-cell level (e.g., Bush & Sejnowski, 1994) and at the macroscopic level of inter-areal connections (Hilgetag et al., 2000; Petroni et al., 2001; Young, 1993), but not, to our knowledge, at the local circuit level as done here. A number of previous researchers have constructed cortical circuit models with the goal of linking anatomy and function (Douglas & Martin, 1991). However, they have mainly focused on properties of one or a few interacting neurons (Bush & Sejnowski, 1994, 1996; Lytton & Sejnowski, 1991) or on bulk properties of the anatomy such as the overall strength and timing of interactions between laminar cell populations irrespective of spatial structure (Douglas et al., 1989; Patton et al., 1992). The details of local circuits aggregated over the scale of millimeters have received comparatively little attention. While horizontal connectivity has been examined in modeling studies of orientation selectivity (Somers et al., 1998; Wörgötter & Koch, 1991), the interaction of this structure with the vertical dimension in the cortex is ignored. Studies that *have* incorporated a vertical component (Fuentes et al., 1996; Lumer et al., 1997) have employed impoverished schemes for horizontal connectivity and made only limited comparisons with physiological data.

METHODS

We begin by defining the class of models the architecture specification we develop is appropriate for, then we describe our process of collating data from the literature and converting the resulting incomplete specification into a full, self-consistent architecture. Next we describe the models we constructed making use of this description – a 3-layer and a 1-layer model constructed through a process of "educated weighted averaging" from the 6-layer architecture specification. Finally we describe the single-cell model we used for simulation. The experimental data we compared the model's behavior with and the results of that comparison are covered in the Results.

Assumptions and Focus

We chose to focus our review of data on cortical circuitry on details generally just above those that would be suitable to capture using compartmental cell models. This was partly in order to reduce the anount of anatomical data to be reviewed as well as to determine how reports should be analyzed. Additionally, given

present constraints on computational resources, it would allow a reasonable facsimile of the neocortical circuitry above the single-cell level to be simulated across a reasonable spatial extent of neocortex. As discussed in the Results section, this was essential to allow a proper comparison to physiological data bearing on architectural parameters, because of the large width of many axonal arbors.

We made no distinctions between characteristics of cells below the level of a population – the category (roughly, morphological type; see below) and layer of occurrence of a cell was in most cases assumed to determine its connectivity properties completely. This approach places emphasis on the "statistical" properties of neocortical architecture in the sense of Braitenberg & Schüz (1991). Accordingly, the structure of the connection "weights" between cells was assumed to depend only on the pair of types involved and the distance between them. While it is believed that much of the *computational* functionality associated with neocortical networks depends upon structure finer than this (i.e., the synaptic weight patterns), there is little evidence that the *dynamical behavior* at a coarser level does. Furthermore, it is thought that this structure arises in many cases through experience and so it is not a fundamental property of the architecture itself.

Regarding the connections between populations, we ignored the dendritic location of synapses, aside from noting a distance category (proximal, middle, or distal) and, in the case of pyramidal cells, the dendritic compartment (basal, apical, or oblique). This information is sufficient for modeling the approximate strength and time course of an input's effect on a post-synaptic cell, but not for representing spatial intradendritic interactions between inputs. We also chose to simplify or ignore a number of details pertaining to axonal arbors, particularly patchiness and other asymmetries. Again, some of this structure may originate during activity-dependent development, and in any case we were aiming for an improvement over existing models, not a completely detailed simulation of biology.

Regarding the cortical laminar structure, we chose to entirely ignore the vertical dimension *within* each of the six layers and represent them abstractly as two-dimensional sheets. Although this rests upon the reasonable assumption that the anatomical variations that mark the different layers reflect commonalities in structure and function within layers as much as differences between them, it does represent a structural simplification.

Finally, although the neocortical tissue shares common architectural principles across different areas and mammalian species, there are variations. While we wanted to collect information on the dimensions and ranges of variation, we also wanted to be able to compare models based on our data collection with physiological experiments carried out in slice preparations of rat somatosensory cortex. Therefore, while we examined data from multiple areas and species, we preferred values from rat somatosensory cortex (parietal koniocortical area/primary somatosensory cortex/Sm-I/Par1 (Zilles, 1985)) where there were differences. In general, the main roles of data from other regions were to serve as checks on the degree of variation, to corroborate those findings based on only a small amount of data in the rat, and to support assumptions made regarding general anatomical constraints.

Gathering and Summary of Anatomical Data

The immediate goals of the data-gathering enterprise were to determine a suitable set of cell classes, broken down by morphological type, layer, and, where necessary, connection properties, and to collect as much information as possible on the distributions of and interconnections between the classes. The former kind of information would specify the rows and columns of a connectivity matrix, and the latter the entries. After collecting the data, we would apply constraint satisfaction to fill in and tune the values.

We began by noting the numbers of excitatory and inhibitory (GABA-positive) cells in each layer within columns of rat primary visual and somatosensory cortex reported by Beaulieu (1993). Table 1 lists averages for these two koniocortical areas (values were similar in both). Overall, inhibitory cells made up 14.5% of the total population of 90,000 cells per square millimeter of cortical surface. For a model incorporating inhibitory and excitatory cells in multiple layers, Table 1 could be used directly to determine the proportions of each cell type to assign to each layer. For our purposes, it served as a source of constraints on the total sizes of further subpopulations defined by morphology and connectivity.

TABLE 1 ABOUT HERE

Excitatory (Pyramidal and Spiny Stellate) Cells

Information on pyramidal cell morphology was taken from studies of rat primary somatosensory cortex (dendritic and local axonal arbors) and primary visual cortex (dendritic spine counts). Note, we include the *spiny stellate* cells of layer IV under the term "pyramidal"; they were treated as a separate cell class throughout, but in most of their properties aside from gross dendritic morphology they are similar to pyramidal cells.

Zhang & Deschenes (1997), Gottlieb & Keller (1997), Lubke et al. (2000), and Elston et al. (1997) intracellularly stained individual cells in rat Par1 with biocytin, allowing full visualization of dendrites and axons. We reduced their axon arbor data to a percentage-diameter format suitable for specifying the density and extent of connections to other cells. For example, one layer III pyramidal cell class had the following reduction: 65% (1500 μm) in II/III, 5% (600 μm) in IV, 30% (900 μm) in V. Pyramidal cells in each layer were divided into one of from 1 to 5 subclasses based on their axonal arborization pattern.

Where quantitative bouton distribution data was not available from these sources (most of the cases), the percentages were determined by visual examination of scatterplots of bouton locations for the layer VI pyramidal cells and examination of the profusion of axon branches for the layer II-V pyramidal cells. Studies have shown that bouton distribution is relatively even along all collateral branches of an axon in monkey neocortex (Amir et al., 1993), validating length as an estimate of output distribution. Douglas et al.'s (1995) analysis of bouton distribution for a cat striate cortex layer II/III pyramidal cell and a layer IV spiny stellate cell arrived at similar conclusions.

Intracellular injection data on individual pyramidal axon arbors is also available for areas 17 (Hubener et al., 1990; Martin & Whitteridge, 1984), A1 (Ojima et al., 1991, 1992), and 4γ (Kang & Kayano, 1994; Keller &

Asanuma, 1993) in the cat, and areas V1 (Callaway & Wiser, 1996; Wiser & Callaway, 1996) and M-I (Ghosh & Porter, 1988) in the macaque monkey. There is also extracellular injection data on composite arbors for areas 9 and 46 in the macaque (Levitt et al., 1993). In most cases, including rat Par1, the arborizations display three general characteristics (see Figure 1):

- Terminal distribution remains largely (usually $\sim$70%) within the compartment of the cell soma – either superficial (layers I–III), middle (layer IV), or deep (layers V-VI).
- In a given layer, some cells give rise to wide arbors stretching over distances of more than a millimeter, while other cells have narrower arbors of much less than a millimeter range.
- The widest portion of a cell's arbor remains within the compartment of the soma. For example, in macaque area 9, axons from cells in layers II and III extend over a 6.9 mm diameter in superficial layers but only 2.7 mm in deep, while axons from cells in layers V and VI stretch over 3.9 mm in deep layers but only 2.5 mm in superficial layers.

FIGURE 1 ABOUT HERE

Both sets of superficial pyramidal cells (layers II and III) are similar to each other in their axonal arborizations, as are both sets of deep pyramidal cells to each other. This fact was used later in reducing the number of cortical layers for a simplified model.

Regarding the contacts made by pyramidal cell axons, counting studies in rodents have found that in most cases between 70–90% of pyramidal axon synapses contact dendritic spines (Elston et al., 1997; Johnson & Burkhalter, 1996), with the rest being contacts on both smooth and spiny dendrites. Variation has been observed in this characteristic among pyramidal cell classes contacting different external targets, such as ipsilateral cortical areas, contralateral areas, the thalamus, and the striatum (White, 1989), but this type of variation fell below our threshold for incorporation, both because we were not distinguishing amongst the various pyramidal subpopulations within a layer in terms of input they receive (so there aren't likely to be differences in the activity of the different cell classes), and because the available data on this subject is patchy. We therefore took a median value of 90% spine or spiny shaft, 10% smooth shaft as our baseline, and left this parameter to be further refined during the constraint satisfaction phase.

The distribution of pyramidal cell dendritic input is better known than the case for axonal output. Larkman (1991a) reported numbers of spines in different layers for individual reconstructed pyramidal cells, allowing accurate specification of dendritic arbors in the format given for axons above. Table 2 summarizes the compiled information on axon and dendrite arbors.

TABLE 2 ABOUT HERE

Inhibitory inputs are located mainly on the proximal dendrites and soma. The review by DeFelipe & Farinas (1992) provides a thorough quantitative description of these inputs broken down by type and location. Table 3 summarizes the data for the rat reported there, for both inhibitory and excitatory types. The sources of each of these types of input will be discussed below.

TABLE 3 ABOUT HERE

Inhibitory Cells

Inhibitory cells in the cerebral cortex have been classified by a number of criteria including axonal/dendritic morphology (e.g., Prieto et al., 1994), neurochemistry (Conde et al., 1994), and physiology (Connors et al., 1982). In general, the morphological classification tends to be finer than the other two, in the sense that neurochemical and physiological categories often – though not always – contain the members of multiple morphological categories as strict subsets (e.g., Gabbott et al., 1997). For this reason, as well as the fact that our study was primarily focused on the effects of spatial characteristics of cortical connectivity, we used a morphological classification – that given by Jones & Peters (1984) – as the primary basis of our data collection.

This yielded 11 cell classes (each occurring in one or more layers), for which we gathered information, as we did for pyramidal cells, on the extents of their dendritic and axonal arbors, the proportions of synaptic contacts they make on spines, smooth shafts, spiny shafts, and other cellular components, and, where possible, their numbers and the proportions of the inputs they receive on distal and proximal dendrites from various sources. As described above, we utilized the literature on multiple areas and species in supplementary and corroborative roles relative to data on rat koniocortex.

The classification of inhibitory cells and references used for each type is summarized in Table 4, together with their layers of occurrence and the types of neural processes they provide input to and in what proportions. Note that the only sources of inhibition of inhibition are basket cells (which inhibit other basket cells only (Kisvarday et al. 1993)), the Small Neuron of Layer I (which inhibits only other layer I inhibitory cells since its axons do not leave the layer), and bipolar cells (which inhibit other inhibitory types in layers II-VI; Gonchar & Burkhalter (1999); Peters & Harriman (1988)).

TABLE 4 ABOUT HERE

Arborization data is summarized in Table 5, for layer III only (the full table, available through `http://zakros.ucsd.edu/ãrobert/CorticalData/`, contains 37 rows). Information on the numbers of each cell type was only rarely available, and we describe how we estimated these values below in the section on estimation.

Note that we exclude the *double bouquet cell* category in Jones & Peters (1984) because no clear examples of these have been published for the rat (although related cells may exist amongst the bipolar cell population – Somogyi & Cowey (1984); see also Meskenaite (1997)). Also, *basket cells* are smaller in rats than cats or monkeys (see Discussion).

TABLE 5 ABOUT HERE

Table 4 lists three cell types – bipolar, Cajal-Retzius, and the Small Neuron of Layer I – as providing $GABA_B$, hyperpolarizing inputs to pyramidal cells, as opposed to the more common $GABA_A$, shunting type. Although $GABA_B$ synapses are known to have a significant impact on pyramidal cell physiological activity by their tell-tale hyperpolarizing effects (Connors et al., 1988; Douglas & Martin, 1991; Shao & Burkhalter, 1999), and their effects on epileptic activity (e.g., Vergnes et al. (1997); see below), very little is known about the anatomical sources of $GABA_B$ inputs in the neocortex, and we came up with our list through the following reasoning.

First, on the basis of experiments in the rat suggesting that separate inhibitory cell subpopulations are responsible for $GABA_A$- and $GABA_B$-type effects on pyramidal response (Benardo, 1994), we eliminated basket, spiderweb, and arcade cells from consideration as potential sources of $GABA_B$, since they all provide somatic inputs which are putatively $GABA_A$ (Tamas et al., 1997). Then we eliminated Martinotti and superficial plexus cells, which both provide layer I inputs to pyramidal cells, because of Vogt's (1991) report that that lesions of sub-layer I cortex affect $GABA_A$ but not $GABA_B$ receptor density in layer I. The only other possible source of the $GABA_B$ inputs in layer I is the Small Neuron. As to the $GABA_B$ receptors in the lower layers (Eder et al., 2001), chandelier cells provide only axo-axonic inhibitory inputs, which are of the shunting, $GABA_A$ type (Buhl et al., 1994). This leaves only the ascending/descending-type cells and bipolar cells. Bipolar cells colocalize neuropeptides (Jones et al., 1987) and possess several other characteristics differentiating them from other inhibitory types, whereas little is known about the ascending/descending type. We chose, therefore, to assume that the bipolar cell provides $GABA_B$ input but the ascending/descending cell does not. The arborization patterns of these two cells are both of the tall, narrow type (see below), so that the effect on activity dynamics in a model from switching the $GABA_B$ from bipolar to ascending/descending cells is not likely to be significant.

Refinement of Specification through Constraint Satisfaction

After the first phase of gathering anatomical data, we had a list of cell populations within each layer, together with complete information on the spatial extents of their dendritic and axonal arbors and incomplete information on the connections each made. In the next phase, we applied constraints to estimate the population sizes and numbers of outputs of inhibitory celltypes in each layer. The methods used varied from celltype to celltype, depending on which information was available, but in most cases the number of pyramidal cells in each layer (Table 1) and the numbers of inputs of various types they receive (Table 3) served as a starting point. We estimated in two stages, first computing the total population and average output characteristics of each celltype across all layers, then refining these to produce individual estimates for each layer.

Both sets of estimated values, together with the data points they were based on and the other data we gathered constituted a collection of hierarchically interrelated and possibly contradictory parameter values based directly and indirectly on observation, sometimes involving assumptions. In order to ensure complete consistency between interdependent values and to allow those more certainly known to own a

greater share in the determination of the others than vice versa, we carried out an iterative computational optimization process that will be described subsequently.

Overall Population Densities

Henceforth we use the term population *density* to refer to the number of cells of a given type beneath a given area of cortical surface, taken to be 1 square millimeter unless otherwise stated. We estimated the total population in all layers for each celltype as follows.

Pyramidal: The density of pyramidal cells was taken from Table 1.

Chandelier: In superficial layers, these are known to contact 300-400 pyramidal cells, while pyramidal cells are known to receive contacts from 3-5 chandelier cells (DeFelipe & Farinas, 1992; Peters, 1984; Somogyi et al., 1982) implying approximately 1 chandelier per 100 pyramidal cells. In deeper layers, pyramidal cells receive approximately half as much axon initial segment input, implying 1 chandelier per 200 pyramidal cells.

Basket: In superficial layers, pyramidal cells get approximately one third of their somatic inputs from basket cells (Peters & Harriman, 1992), or about 70 for noncorticothalamic cells, baskets send approximately 25% of their output to pyramidal somas (White, 1989), and we assumed 10,000 outputs per basket (an estimate based on overall GABA synapse-to-cell ratios in rat 17 (Beaulieu et al., 1994)): implies 1 basket per 36 pyramidal cells.

Bipolar: Immunocytochemical methods estimate bipolar cells make up 2–5% of the entire population in the rat (Gabbott et al., 1997a); assuming half of bipolar output is to spines and applying constraints from inhibitory spine input (need 195 per pyramidal cell after basket, 177 after layer I input – see below), this implies 1 bipolar per 29 pyramidal cells.

Spiderweb, Arcade: These cells have similar arborization radii and jointly provide two thirds of the somatic inputs to superficial pyramidal cells (Peters & Harriman, 1992); we assumed 10,000 outputs per cell, of which one third go to pyramidal cell somas (estimate): implies 1 spiderweb and 1 arcade for every 48 pyramidal cells assuming equal number of each.

Ascending/Descending, Superficial Plexus: To make up the remainder of inhibitory shaft inputs to pyramidal cells, need a total of 369 (= 1100 - 731 (187 (Basket) + 177 (Bipolar) + 280 (Spiderweb, Arcade) + 87 (Layer I – see next))), assumed 10,000 output per cell: implies 1 ascending/descending and 1 superficial plexus cell per 54 pyramidal cells assuming an equal number of each.

Cajal-Retzius, Small Neuron of Layer I: Total layer I inhibitory cell population is 1 for every 142 pyramidal cells across all layers (Table 1); we assumed an equal number of Cajal-Retzius & Small Neuron, 10,000 out per each cell (Cajal-Retzius contacts shaft only, Small Neuron contacts 50% shaft and 50% spine), implying 52 shaft contacts and 18 spine contacts per pyramidal cell provided by 1 Cajal-Retzius and 1 Small Neuron per 284 pyramidal cells.

Martinotti: Very little information is available; we assumed the proportions and outputs were similar to Small Neuron of layer I but 100% to shaft: implies 1 Martinotti per 284 pyramidal cells (total of 35 shaft contact per pyramidal).

Ovoid: To approximately make up for absent chandelier and layer I inhibitory influence in layer VI, need 310 (= 20 (chandelier) + 105 (Cajal-Retzius, Small Neuron, Martinotti) + 185 (superficial plexus)) inputs per pyramidal in this layer: implies 1 ovoid per 32 pyramidal cells in layer VI, or 1 per 108 pyramidal cells overall.

Laminar Densities

The distribution of the overall populations of each celltype across the layers was determined as described below. In the interests of brevity we do not provide the specific numbers in each case, however they may be obtained from the web site at `http://zakros.ucsd.edu/~arobert/CorticalData/`.

Pyramidal: While the total number of cells in each layer is known (Table 1), there are typically several different arborization types in a layer. We could not find data on the proportions of these for rat primary sensory cortex, nor for any case aside from some layers in Macaque primary visual cortex (area 17), which is not believed typical of cortical areas. Therefore, the assumption was made that each arborization type occurs with equal frequency.

Chandelier, Basket, Spiderweb, Arcade: It was assumed that the pyramidal cells these contacted were only those with somas in the layers of their axonal arborization; since chandelier, spiderweb, arcade, and small basket cell axons arborize only in a single layer (to a first approximation), their cell distribution is completely determined by the estimated number of outputs they provide and the number of inputs the pyramidal cells were estimated to receive from them. For the large basket, it was necessary to distribute outputs between the layers that their arbors spanned so that pyramidal cells there received the appropriate total amount of basket input from all sources; these problems were underdetermined and so the relative proportions were further constrained to be as close as possible to those of the pyramidal cells in the layers.

Bipolar, Ascending/Descending: These cells were the most complex because of their vertically elongated arborizations. The primary consideration in distributing these types was to distribute their output evenly over the pyramidal cells in each layer given their known arbor shapes. Additionally, there is some immunocytochemical evidence that the distribution of bipolar cells does not follow layer pyramidal cell proportions but preferentially occupies layers II and V. Initial distribution was done according to these loose constraints while trying to match the overall inhibitory distribution as closely as possible.

Superficial Plexus: These cells exist in layers I-IV and send their axonal arbors upwards. Without the superficial plexus innervation, any given pyramidal in layers II-V would be short of inhibition relative to those that do receive it, therefore it was assumed that these arbors contact the apical dendrites of all of these pyramidal cells when they reach the upper layers. (Layer VI possesses additional local inhibitory celltypes that make up for this missing influence – see below.) With this in mind, superficial plexus cell bodies were distributed in I-IV according to overall cell proportions in these layers.

Cajal-Retzius, Small Neuron of Layer I: These cells occur only in layer I, so no distribution needs to be determined.

Ovoid: This type occurs only in layer VI, so no distribution needs to be determined.

Computational Optimization of Population and Connectivity Parameters

As stated earlier, the directly and indirectly obtained (estimated) parameters resulting from the operations thusfar were lastly subjected to an iterative computational optimization process in order to ensure complete consistency between interdependent values and to allow those more certainly known to determine adjustments to those less certainly known. The primary idea of the optimization method was to take the assumed numbers of outputs from each class of cell, and combine this with both the axonal and dendritic arborization data and estimates of the density of occurrence of each class to estimate the number of inputs of various types that each cell class would receive. These numbers were then compared with the numbers of inputs known from the data (where they *were* known), and the resulting difference was used as the input to a delta rule for adjusting both the output and input parameters, and the density estimates.

For example, suppose that layer III pyramidal cells are currently estimated to send 90% of their output to spiny dendrites, putatively belonging to pyramidal cells, and of this, 40% is known to stay in layer III, judging from the percentage of the axonal arbor there. On the other hand, the dendrites of layer III pyramidal cells themselves make up 70% of all the eligible spiny dendritic surface within layer III, based on the dendritic arborizations and densities of pyramidal cells in layer III and all other layers. Thus, the estimated input from layer III pyramidal cells to other layer III pyramidal cells is on the order of $0.90 \cdot 0.4 \cdot 0.7 \cdot 1.0 \cdot 4000 = 1008$, where the 1.0 is the source-to-destination density ratio, and the 4,000 is an anatomical parameter, the number of local outputs per pyramidal cell. (It is recognized that the implicit assumption here, that connections are made in proportion to the amounts of axonal and dendritic surface coming into contact, may not be accurate for all cases (White, 1989), but it is a reasonable starting point.) The same calculation is performed for the pyramidal cells in other layers to determine the total excitatory input to

layer III pyramidal cells, and the total is then compared to the currently estimated number of local excitatory inputs to layer III pyramidal cells based on spine counts, say 4,000. If it is less, all parameters contributing to the pyramidal input will be revised upwards in proportion to their contributions and in inverse proportion to the a priori confidence in their starting values to the extent that the adjustment would move them away from these values. If it is greater, the contributing parameters will be revised downwards. Simultaneously these calculations are carried out for all classes of cells at each step, and the final adjustments result from the summed contributions from many different comparisons. A synchronous update method is used.

The actual algorithm applied was somewhat complicated by the fact that constraints arise at multiple levels of granularity. For example, for inhibitory cell classes, there are both estimates of the numbers of specific classes of cells and estimates of the total number of all inhibitory cells. This type of case was handled by first applying the delta-rule adjustments independently at both levels, and then applying a hard normalization afterwards so that the lower-level (finer-grained) values totaled up properly to the higher level value. The net effect of this introduced a bias giving more weight to the higher level values, but these tended to be known with greater certainty than the lower level ones anyway.

Details on the parameters used, the relations between them, and the update algorithm are in Appendix B. We tested the optimization implementation on a number of simple cases with just 2–4 cell populations and different missing or purposely maladjusted parameter values to ensure that it was capable of reconstructing sufficiently constrained data values.

For actual data, the input/output and distribution parameters represented in the network typically relaxed to a stable state after 10–100 steps depending on the rate parameter. In reaching such states, most of the initial values did not change more than 10%. This was the case even when an annealing process was applied in which all values are periodically perturbed by a noise value whose amplitude decreased over the course of the optimization (Van Laarhoven & Aarts, 1987), and in these cases, the standard deviations of the final settings over multiple runs were all less than 10% of their values. This is interesting because it suggests that the estimated values occupy a relatively flat, wide minimum within the space; refinements in the detail of the available anatomical data may not change the computed connectivity appreciably.

A portion of the final distributions and connectivity (for layer III only) is shown in Table 6.

TABLE 6 ABOUT HERE

Model Construction

The architectural specification at this point consisted of 51 cell populations distributed across 6 layers and making 1062 connections out of a possible 2601 (many of these involved very small numbers of synapses and may not occur in the real system due to competitive elimination). We desired to test the accuracy of the specification by comparing the behavior of models instantiating it with neurophysiological experiments in rat neocortical slices. The overall structure of the models we used was a stack of square lattices of cell units, each lattice representing a population of a particular kind of cell within a particular layer (Figure 2).

Distance in lattice units corresponds to lateral distance within the cortex related by a scaling parameter that differs from population to population depending upon the densities with which the actual and model cell types occur. Connections are made within and between lattices according to the derived specification data.

FIGURE 2 ABOUT HERE

While it would be possible to construct a very complicated, 6-layer model straight from our architectural specification, it would be highly unwieldy. We actually experimented briefly with such an approach, but soon elected to simplify the specification successively to 3- and 1-layer versions to be used for constructing models. This process is described below. It was also necessary to address several practical issues relating to model construction. We discuss these first.

Density Reduction

The rat primary somatosensory neocortex contains about 10^5 neurons and 10^9 synapses per mm^2 surface area, however many of the cell arbors extend for substantial fractions of a millimeter or more. Modeling several mm^2 of cortex of this density would have been out of the reach of present computational resources – yet necessary to capture the range of spatial interactions. Therefore we reduced the total density of cells and the number of connections by a scaling factor while leaving arbor sizes unchanged, as done in other neural modeling work (e.g., Wilson & Bower, 1989; Wörgötter & Koch, 1991); synaptic weights were increased in partial compensation (see below and Appendix A). Typically, we reduced inhibitory populations by a lesser factor than pyramidal populations, because otherwise the densities of certain inhibitory celltypes would have been too low to ensure output coverage to all pyramidal cells (i.e., inhibitory cells would be spaced further apart than their axonal arbor diameter plus the pyramidal cell dendritic arbor diameter). We did not, however, attempt to model local variations in cell density over the cortical surface such as are seen, for example, in the rodent barrel cortex. The scaling factors we used were: Pyramidal:30, Chandelier:8.3, Basket:16, Cajal-Retzius:12, Small Neuron:12, Martinotti:12, Bipolar:14, Spiderweb:19, Arcade:19, Ascending/Descending:17, Superficial plexus:17, Ovoid:16. (Inhibitory scaling was allowed to vary somewhat for the conveniences of having each type provide the same number of output connections, and having pyramidal cells receive a whole number of connections in from each type.) The scaling used afforded simulation of the cortex with about 3,400 model cells per mm^2.

This reduction implies that a model cell in some sense represents a population of biological cells centered around its location. However, the response properties of the model unit are still those of a single cell – hence, it is more accurately thought of as representing a 'slice' of the biological network, or a 'typical' cell. Because its *synaptic output* has a stronger effect on other cells than in biology, it should be thought of as representing the effects of a population of cells with similar activation levels. Thus, the model cells are equivalent to real cells, but model connections are equivalent to sets of connections between populations. Note that, because spiking cells are used, this implies a high degree of synchrony in the equivalent states to the model in a more detailed system; this cannot be avoided in a density-reduced spiking simulation, but we lessened the

effects by using weaker synapses than strict scaling would imply in order to preserve input variance (see next section and Appendix A).

Connection Weights

This interpretation means that a model cell should contact all of its neighbors rather than a subset as in the real cortex (Braitenberg & Schüz, 1991), and connection *weight* in the model represents the effects of connection *probability* in the cortex. Connection weight was therefore determined in two stages:

1. Scale the peak conductance values for equivalent synapses in the biological cortex by the density reduction factor, and readjust for variance preservation (details in Appendix A).

2. Apply a further scaling factor to compensate for the disparity between the number of cells contacted in the model (typically all neighors within range, usually 200–500) and the number that would be contacted if the number of outputs of the biological cell was simply adjusted by the cell density scaling factor (e.g., about $5000/30 = 167$ for a pyramidal cell's local connections).

The final weights between pairs of cells also depended on the lateral Euclidean distance between them, reflecting the fact that connection probability falls off as the intersection between the axonal and dendritic arbors decreases with distance between the somas. (Effects of vertical distance within a layer were ignored since layers were idealized as flat sheets.) The probability is also affected by the density function of pre- and post-synaptic elements within the arbors themselves. For axons, the number of boutons per unit length of axon appears to be generally constant throughout an arbor (Amir et al., 1993; Hellwig et al., 1994), however, details of the branching function are not well known. Paldino & Harth (1977) provide virtually the only quantitative analysis of pyramidal axon terminal distribution in neocortex, but their data must be regarded as approximate, as they employed the Golgi stain in adult animals, known to stain myelinated axons incompletely. They found that the lateral distribution of collateral terminals falls off approximately exponentially with distance from the soma, with a length constant of approximately 100 μm. That is, the density of terminals at a radial distance (measured in μm) $r \propto \exp(-r/\lambda) = \exp(-0.01r)$.

We assumed that the form of this function would also describe the overall distribution of boutons on the complete tree, but that the length constant was higher. Typically we used a constant λ = 625 μm, for which density falls off by about half at r = 400 μm, and by 80% at 1 mm. Arbors were truncated at the anatomical maximum widths rather than smoothly falling to zero. The sum of the truncated function over the grid of cells connections were to be made to was normalized before applying it to the weights.

We took account of the effects of dendrites simply by adding dendritic arbor radius to axonal radius to determine the maximum connection distance. The inaccuracy introduced by this treatment was minor, because the typical radii of dendritic trees are much smaller than that for axons, sometimes by an order of magnitude for pyramidal cells, so that the falloff characteristics for axonal arbors will dominate connection probabilities. We did not model dendritic geometry, but did group inputs into proximal, middle, and distal classes based on factors such as whether a given input is known to be generally proximal (e.g., inhibitory synapses from basket cells), or whether it must necessarily contact distal portions of the tree (e.g., synapses

from an axonal arbor in layer II onto a layer V pyramidal cell). Different peak conductances and time constants were used for the different classes.

Edge Considerations

At the edges of the sheet, cells sent and received fewer connections. We did not use periodic boundary conditions (as often employed in similar models) because we compared our networks to slice preparations, in which connections are also truncated.

Three Layer Model

The 3-layer model we built within this framework was intended to simplify the architecture from the 6-layer specification while preserving the most important features of its laminar structure. The three layers in this model represented superficial (layers II-III), middle (IV), and deep (V-VI) compartments. Because pyramidal cells in both superficial layers II & III and also those in deep layers V & VI both share most of their arbor characteristics (see Figure 1 and accompanying text), and layer I contains mainly neuropil whose effects can be subsumed by connections amongst the other layers, we judge this reduction to preserve the most important characteristics of the laminar architecture.

Each of the three layers contained a single pyramidal cell population whose arborization and connectivity characteristics were an average of those of the corresponding constituent populations in the 6-layer specification, weighted by the population sizes. For inhibitory cells, a similar strategy was employed, except that first we reduced the number of morphological classes from 11 to 4 as follows:

Small These cells have narrow axonal and dendritic arbors within their own compartment only and provide $GABA_A$ inhibition to pyramidal cells. They replace the chandelier, small basket, spider-web, and arcade cells in the full model.

Wide These cells have moderate dendritic and wide axonal arbors within their own compartment only. They provide some inhibition to other inhibitory cells. They replace the ovoid and medium basket cells in the rat cortical model and would also replace large basket cells in models of cat or monkey cortex.

Bipolar These cells, taken straight from the 6-layer specification, have narrow localized dendritic and axonal arbors spanning vertically across compartments. They provide both $GABA_B$ and $GABA_A$ inhibition to pyramidal cells, as well as $GABA_A$ inhibition to other inhibitory cells.

Ascending/Descending These cells were also taken straight from the previous model and have narrow dendritic and axonal arbors spanning across compartments. They provide $GABA_A$ inhibition to pyramidal cells.

Each type occurs in one or more layers. The axonal and dendritic arborization characteristics in 3-layer model are listed in Table 7. The number of cell populations was reduced from 51 in the 6-layer specification to 13, and the number of connections between populations was reduced by about 80%. The cell distributions and interconnections, given in Table 8, were determined by first estimating them by averaging the scaled values from the 6-layer specification for the populations they replace, then applying the same computational optimization process as before to fine-tune them. Figure 3 displays all the celltypes in the 3-layer model to scale.

TABLE 7 ABOUT HERE

TABLE 8 ABOUT HERE

FIGURE 3 ABOUT HERE

Single Layer Model

The 1-layer model was constructed using two laterally-connected cell populations, pyramidal and inhibitory. In some implementations the pyramidal population was subdivided into bursting and regular-spiking cells, while in others only regular-spiking cells were included. The arborizations for the connections were set to the weighted average of the entire classes of connections (e.g., pyramidal-inhibitory) they replaced in the 6-layer specification. The pyramidal cells had dendritic and axonal arbor radii of 150 and 250-1000 μm respectively (see below), while the inhibitory cells had radii of 100 and 150 μm.

One version of this network contained only $GABA_A$ inhibitory synapses, while the other version also contained $GABA_B$ at a narrower (40 μm) radius in a similar proportion to that in the laminated networks (from the bipolar cells).

Because of the variations in axonal arbor diameters between different pyramidal cell classes (see above), pyramidal connections in the model (to both pyramidal and inhibitory cells) were made with a composite structure: 50% over a 250 μm radius, 20% over a 500 μm radius, and 30% over a 1 mm radius (see Figure 1). This complex lateral interaction function (henceforth, "Baseline") is often further collapsed into a single exponentially-decaying connectivity function (Golomb et al., 1996; Wilson & Cowan, 1973). We studied the functional effects of accomplishing this in three different ways (Figure 4):

Fit: A single set of connections was made over the longest distance (1000 μm) but with a faster exponential decay constant fit so that the overall density falloff resembled the composite one as closely as possible (by a least-squares measure).

Average: A single set of connections was made over the weighted average distance of all three sets in the composite (530 μm), but no effort was made to fit the exponential decay to match the composite; the same decay as for each of the composite components was used instead.

Short: A single set of connections was made over the shortest distance of the three composite components (250 μm), also with an unfit exponential decay.

FIGURE 4 ABOUT HERE

Cell Model

Cells

Cortical cells were modeled by single compartment conductance-based units similar to those described in Wilson & Bower (1989). This model captures basic temporal behavior of real cells and affords comparison to

physiological experiments without great computational expense. The equation for the evolution of membrane potential in a cell with membrane capacitance C_m, membrane conductance g_{leak}, resting potential E_m, and membrane potential V_m is:

$$C_m \frac{dV_m}{dt} = (E_m - V_m)g_{leak} + \sum_{k=1}^{n_{syn}}[(E_k - V_m)g_k] + \sum_{l=1}^{n_{chan}}[(E_l - V_m)g_l]$$

Here, E_k, g_l, etc. represent synapse and channel Nernst potentials and conductances. Cell parameters C_m and g_{leak} were determined based on physiological measurements that have been used in previous modeling work (see Appendix A).

Synapses

If the membrane potential reached a threshold in a unit, it was reset to the resting potential and a spike event was propagated with a delay to synapses on other cells, the effects of which were modeled by alpha-function conductance changes (Jack et al., 1975). The g_k of a synapse after being activated at $t = 0$ is:

$$g(t) = g_{peak}\frac{t}{\tau}e^{(1-\frac{t}{\tau})}$$

where g_{peak} is the peak conductance, which occurs at time $t = \tau$. To determine these parameters, we ran an initial set of calibrating simulations in NEURON (Hines & Carnevale, 1997) using a single multicompartment reduced model of a layer V pyramidal cell (Bush & Sejnowski, 1993). For each of a small number of contact location categories (somatic, proximal, middle, distal), synaptic input was provided to an appropriate receptor on that portion of the dendrites, and the resulting effects measured at the soma were used to determine the parameters for that type of synapse in the single-compartment model (which was *not* simulated with NEURON – see below). Glutaminergic AMPA, $GABA_A$, and $GABA_B$ synapses were modeled, with τ of approximately 0.5-1, 0.5, and 20 msec respectively. (After filtering through membrane capacitance, these generated waveforms of effect on membrane potential with times to half-decay of approximately 2.2, 1.5, and 70 msec respectively.) The peak conductance was scaled as discussed under "Connection Weights" near the end of the Methods section. The effects of local dendritic saturation (e.g., Bush & Sejnowski, 1994) are not accurately represented by this model; however, the general time courses of the different input classes are. The parameters of the cells and synapses used are summarized in Appendix A.

In most of our simulations, we did not distinguish AMPA from NMDA receptors because of uncertainty in the subclasses of connections they implement – and also because we wanted to keep the complexity of the model to a manageable level. We did investigate the effects of distinct NMDA channels in a few simulations of the 1-layer model (see Appendix A and Results). Here, 20% of the excitatory-excitatory AMPA connections were converted into NMDA synapses, only triggerable at $V_m \geq -45$ mV, with $\tau =$ 10 msec (Jones & Baughman (1988)).

The firing thresholds of all cells were set according to a Gaussian distribution with μ = -40 mV and σ^2 = 2 mV. The variation was intended to capture known biological variability (not necessarily of just threshold) at both the cellular (McCormick et al., 1985) and local network levels (Tsau et al., 1998), in order to compensate for the overly regular connection structure. In some simulations a small noise current was

also injected independently into each cell at each timestep, however this had no symmetry-reducing effect beyond what the threshold variability already produced.

Conduction delays were usually set based on a Gaussian distribution with $\mu = 1.2$ msec and $\sigma^2 = 0.2$ msec, independently of distance. Although we experimented with grid distance based delays, it would require detailed knowledge of which connections employ myelination and which do not to do a proper job of this. By using a distance-independent function, we in effect assumed that connections over longer distances are more likely to be myelinated than those over short distances. Anecdotal observations such as the fact that basket cell axons are often myelinated while spiderweb axons are not support this view.

Channels

Although finer categorizations exist, cortical cells in the rat are generally considered to fall into three broad classes based on intrinsic physiological response properties: regular spiking (RS) pyramidal, intrinsically bursting pyramidal (IB), and fast spiking (FS) inhibitory (McCormick et al., 1985; Prince & Huguenard, 1988). Additional conducting channels were included in the cell model to mimic the effects of currents differentiating these classes. Rather than modeling the activation kinetics of the channels involved with additional differential equations (e.g., Lytton & Sejnowski, 1991), which would have required a much smaller timestep, the conductances of AHP potassium and burst calcium channels were controlled in a finite state automaton-like fashion at each timestep utilizing present and recent-past membrane potential plus a set of state variables (methods summarized in Appendix A). This resulted in piecewise approximation of the true kinetics but then allowed numerically stable simulation at a timestep of 10^{-4} sec using a fourth-order Runge-Kutta method (Press et al., 1992). Reducing the timestep by an order of magnitude never caused simulation results to change appreciably. Figure 5 shows plots of membrane potential and spiking behavior in response to current injection for each of the three model cell classes.

FIGURE 5 ABOUT HERE

Simulation Environment

All simulations (excluding the calibration stage) were run on MIPS R4400- and R10000-based Silicon Graphics workstations with 200-256 Mb main memory. They employed special-purpose software (written by the authors in C++, available upon request), implementing networks of single-compartment spiking neurons. Typical running times for simulations described in this paper were within the range of 10 minutes to 2 hours.

RESULTS

The behavior of each of the three models simulated as a 2x4 mm patch containing around 27,000 model cells was compared to data from rat neocortical slices measuring the effects of point stimulation at the

layer VI-white matter border. The physiological data provided information on two aspects of the spread of activity – propagation in the horizontal direction and transfer across the vertical direction, allowing assessment of whether the model's excitability and characteristic lengths of activity spread accurately matched the biology. In both cases, the model replicated experimental results while shedding light on underlying mechanisms.

We cover the horizontally- and vertically-related results in turn, describing first the experimental setup and results, next the stimulation and recording of the model used to simulate the experiment, and then the model's behavior under these conditions. Then the behavior is compared with the experimental results and the effects of manipulations of model parameters are described.

Experimental Results on Horizontal Spread

Two sets of experiments providing data on horizontal activity spread were used, the first by Chagnac-Amitai & Connors (1989a,b), and the second by Langdon & Sur (1990), both performed in rat primary sensory cortex (somatosensory and visual respectively). The experiments were conducted for the purposes of gaining insight into mechanisms of activity propagation in epileptic-like states as well as the structure of local cortical circuitry in general. We chose them for comparison because they involved large numbers of trials and were highly systematic in terms of stimulation and recording methods. We discuss our findings in relation to several other published experiments following the main presentation.

Chagnac-Amitai & Connors recorded local field potentials from a series of 4 electrodes in layers II/III laterally spaced at 0, 600, 1400, and 2200 μm from a brief pulse stimulation point located in layer VI. They repeated their procedure under several different levels of bicuculline-induced $GABA_A$ disinhibition. The setup is illustrated in Figure 6, and the results reflected the following features:

FIGURE 6 ABOUT HERE

CC1: The field potential event had a positive width of 10 msec and a total width of 20 msec.

CC2: Lateral propagation of the field potential event occurred with reliability dependent on disinhibition level; about 20% was sufficient to generate completely reliable propagation. Activity shut down in previously active areas as it spread elsewhere – i.e., the propagation was wave-like. Propagation speeds were in the range of 80-100 μm/msec.

CC3: Regeneration/reflection sites were observed at higher disinhibition levels.

Langdon & Sur (1990) recorded field potentials from a series of electrode placements in layers I-V above a brief pulse stimulation point in the white matter as well as a series of placements in all layers at lateral displacements of up to 2 mm. They did not induce disinhibition in their slices. Their findings reflected the following features:

LS1: There were three main components in the field potential responses above the stimulation site: 'S1', 1-2 msec wide, peaking 3-4 msec after stimulation, attributed to antidromic activation; 'S2', similar but following 3 msec later and repeating at this interval; and 'W1', 50-100 msec wide, peaking at 10-20 msec.

LS2: Both the S2 and W1 components (or sometimes the W1 by itself) were observed at points ranging up to 1.7 mm away from the stimulation (but usually not more than 0.5 mm); the propagation speed was usually around 100 μm/msec.

LS3: Measurement of the lateral distances over which S2 was observed with the same latency as above the stimulation site suggested that excitatory connections drop off sharply beyond distances of 300-400 μm.

Overall, Chagnac-Amitai & Connors mainly observed the long-distance propagation of relatively large, monolithic waves of activity, while Langdon & Sur observed the local spread of a long wave of excitation modulated by a series of shorter, sharper potential events.

1-Layer Model: Stimulation and Observed Activity Regimes

To replicate the conditions in Chagnac-Amitai & Connors (1989a,b), a 1 msec current pulse sufficient to fire cells was applied to the central excitatory and inhibitory cells in the network (radii of 200 μm and 50 μm respectively), and a weaker pulse sufficient to depolarize cells approximately halfway to their thresholds was applied over a wider radius (r = 250 μm and 100 μm respectively). These pulses were meant to imitate the effects of both dendritic and antidromic activation of cells with processes within a sufficiently small radius of the stimulation point in the slice. To replicate Langdon & Sur's conditions, the pulse was applied to the same number of excitatory cells as in the Chagnac-Amitai & Connors case, but fewer inhibitory cells, since they would not have been antidromically activated (see discussion of stimulation of 3-layer model below).

The strength of $GABA_A$ synapses onto both pyramidal and inhibitory cells was systematically varied to imitate the effects of bicuculline disinhibition. Other parameters were varied to a lesser extent (see below).

The differences in model behavior we observed between the stimulation conditions matching Chagnac-Amitai & Connors and Langon & Sur respectively were limited to a slightly greater tendency to excitability in the latter case, both for the 1-layer model and (see below) the 3-layer model. We confine our report from here forward to stimulation under the former set of conditions.

In the network employing only $GABA_A$ inhibition, only two kinds of behavior were usually observed (Figure 7 left, center): a spreading activity zone that lasted up to 20 msec and spread out to at most double the initial stimulation radius before collapsing to quiescence, or an indefinitely growing zone of activity at maximal firing rate that spread through the entire network. The transition on the disinhibition scale between these two types of behavior was relatively sharp, but variation was smooth (in terms of length of time to quiescence/radius of spread and explosion spread rate) within the two regimes. We denote the inhibition level at the transition by the ratio d_c of $GABA_A$ strength at transition (found by a recursive bisection technique) to that at normal baseline.

FIGURE 7 ABOUT HERE

The network additionally employing $GABA_B$ inhibition exhibited the above two regimes plus a third of wave propagation (Figure 7, right), situated in between the other two. In this regime, activity spread in a radial fashion until a critical radius was reached, then it continued in only a subset of directions while extinguishing in the others; the thickness of the resulting wavefront remained constant at this radius but its width could increase apparently indefinitely. (Note, the symmetry was broken by the small variations

in firing thresholds (see Methods).) The thickness in this case varied smoothly with disinhibition level ($GABA_A$ only) but the speed remained constant.

Intermediate behaviors were observed at the boundaries of the regimes – between quiescence and wave propagation there were $GABA_A$ levels for which waves would propagate some short distance with the front shrinking then dying out, and between the wave and explosion regimes there were levels in which most of the network would explode and then decay to quiescence. The actual range of $GABA_A$ levels for which wave propagation occurred depended on several factors (see below).

Comparison of 1-Layer Model with Experiment

The experimental results were reported mainly in terms of local field potentials, which are generated by current flow across the membranes of cells. Current flows can be estimated in the cortex by the method of current source density analysis (Mitzdorf, 1985), which mostly detects synaptic currents and passive return current rather than action potentials. However, current source density does not directly reflect the somatic membrane potential of cells, which is the primary output of our single-compartment model, and many more assumptions are needed to generate current source density values from our simulations. We therefore concentrate on gross properties of the local field potential (or current source density signal) in the slices in our comparisons to model membrane potential. In particular, we focus on first arrivals or peak times of signal at particular distances and not on relative levels of activation.

The comparison of the model with the slice results is as follows.

- Under baseline lateral connectivity, activity events in wave propagation regime (as measured by half-height width of the membrane potential deflection) lasted between 10 and 20 msec, as in CC1 (see Figure 7, right).
- In the quiescence regime, the initial, stimulation-generated membrane potential deflection lasts only 1-2 msec and is followed by a second event about 3 msec later, as in LS1 (Figure 7, left, right).
- Propagation speeds in the wave regime under the baseline (composite) connectivity were in the range of 80-100 μm/msec as those observed experimentally (CC2) (Figure 7, right).
- Propagation speeds in the quiescence regime were also in the range of 80-100 μm/msec, similar to result LS2 (not shown).
- Regeneration sites (CC3) were *not* observed except when the reflection led to explosion.
- The range over which activity appeared to spread in a single synaptic step (LS3) depended on the connection mode employed (see below) but fell between 300 and 600 μm for the most faithful (baseline) mode.

Both $GABA_A$ inhibition level and the alternative pyramidal connectivity patterns strongly affected the speed and range of propagation, as illustrated in Figure 8A. We measured the speed based on time from peak to peak on membrane potential plots between sites 1–1.2 mm apart (see Figure 9) for one run for each pattern/inhibition-level combination (variability over different random seeds was negligible in the cases we examined this).

Overall, speed was lowest for the "Short" method of collapsing to a single exponential, but this was also the most excitable pattern, in that the smallest level of disinhibition was required to bring the network to explosion mode. The reason for the latter is that, since cell output was normalized to the same total strength in each case, longer excitatory connections are weaker to any one spot, making it difficult for suprathreshold activity to spread from a limited initial area. Both the Short pattern and the Baseline condition (for which

50% of the connections are made within the short distance) were more excitable than either of the other two alternate patterns. The combination of strong local and weaker long distance connections was also the most effective in generating a high propagation speed, and the Baseline pattern's speed was closest to that experimentally measured over the range of response levels (Figure 8A).

Propagation speed varied surprisingly little across a range of synaptic strengths (at comparable overall activity levels). In networks with very weak or very strong synapses, speeds had to be measured in quiescence with almost negligible inhibition (otherwise propagation did not go far enough to measure speed), with the result that speeds are artificially high, unhindered by inhibition, or they came exclusively from the explosion regime (Figure 8B).

FIGURE 8 ABOUT HERE

The connectivity pattern also affected the distance over which activity could be monosynaptically transmitted. Langdon & Sur (1990) found (LS3) that strong excitation arrived at all sites within a 300-400 μm radius more or less simultaneously. In the model, this was the case for both the Short and Baseline conditions, however, in the Average condition, simultaneous transmission occurred over longer distances between 600 and 900 μm, and, in the Fit condition, over 900-1200 μm (Figure 9). Despite having a partial local concentration of connections similarly to the Baseline pattern, the smooth continuation to longer distances gave this condition a longer effective wavelength for activity spread.

Because the both the speed and transmission characteristics generated by the Baseline connectivity pattern most closely matched the experimental results, we concluded that the essential feature of this pattern – a composite structure with several characteristic lengths – is responsible for shaping the propagation characteristics in the real cortex.

Effects of Other Parameter Variations in 1-Layer Model

To test whether other factors besides pyramidal connectivity pattern could be responsible for determining these characteristics, we studied the 1-layer model while varying its other connection parameters. We varied each parameter individually over roughly a factor of four, exploring each value for a series of different levels of $GABA_A$ inhibition (Table 9). Whenever the lengths of connections were varied, their weights were normalized so that the total weight remained constant.

TABLE 9 ABOUT HERE

The results in the table indicate that most of the parameters affected the regime transition points, while a few also affected the propagation speed and/or the wave thickness. The strength of excitatory-excitatory synapses had only a weak affect on speed, contrary to earlier observations in models which did not include inhibitory cells (Ermentrout, 1998; Golomb & Amitai, 1997) or relied on inhibitory synapses and post-inhibitory rebounds for the primary transmission mode (Golomb et al., 1996). Decreasing the inhibitory-

excitatory length increased speed (Figure 8C); however lowering it to a point where speed in the short connection condition approached that of the Baseline condition required halving the length to a 120 μm radius (including postsynaptic dendritic distance to cell body). This is considerably less than known anatomical values (Tables 2 and 7). Excitatory-excitatory length had a strong effect on speed when falloff (the connection length constant) was held fixed (Figure 8D), as expected from the effects of connection mode already described. Finally, both inhibitory-excitatory length and $GABA_B$ strength affected wave thickness; however they did not alter the monosynaptic transmission distance discussed above at all (data not shown).

Finally, we ran some simulations in which an NMDA connection was added between cell units (see Methods, Appendix A). We examined a range of total peak conductances from 1–4% of the AMPA total, giving values for total integrated conductance over a single synaptic event of 10–40% of that for the AMPA. We found that, in the lower three fourths of the range, there was little effect other than to make the waves slightly thicker – a result that was also found by Golomb & Amitai (1997) in their simpler model. At the higher end of the range, excitability was increased, and propagation speeds were reduced relative to AMPA-only simulations at the same activity level. Because experiments on neocortical slices have not revealed major excitability-decreases mediated by NMDA antagonists (Hwa & Avoli, 1991), we assume that the lower end of our range accurately models physiological conditions.

In sum, the central role of a multi-tiered excitatory connection mode (i.e., the "Baseline" mode referred to above) in reproducing the experimental results cannot be canceled out by variations in other parameters.

Mechanisms of Horizontal Activity Propagation

The relations between anatomical structure and physiological function that may be inferred from the above results are:

1. Existence of the wave regime depends on an intact $GABA_B$ system, which acts to extinguish long-active parts of an expanding explosion.
2. Propagation speed depends on both excitatory connection length and its density-with-distance structure; longer length gives faster propagation (unless falloff is increased), as does shorter inhibitory-excitatory length. Variation in synaptic strength has little effect.
3. Monosynaptic transmission distance depends on excitatory connection pattern, while wavelength depends on this along with inhibitory-excitatory connection lengths and $GABA_B$ strength.

The first result has some empirical support. Although $GABA_B$ has not received a lot of attention in studies that have attempted to model wave propagation in the cortex (see Discussion), it has been shown experimentally *in vitro* that agonists reduce frequency and duration of spontaneous discharges in hippocampus (Karlsson & Olpe, 1989; Karlsson et al., 1992) and neocortex (Ong & Kerr, 1994). Antagonists have a limited opposing effect to that of the agonists but do not lead to massive discharge in the same way as bicuculline (Karlsson & Olpe, 1989), presumably because the $GABA_A$ conductance is by far the larger source of inhibition. *In vivo*, $GABA_B$ agonists can cause increased burst firing in the thalamus (Caddick & Hosford, 1996), a counter-effect which may be responsible for relatively weak effects of systemically-applied $GABA_B$ agents on convulsant activity (Badran et al., 1997). Indeed, Vergnes et al. (1997) demonstrate a direct convulsant

effect of $GABA_B$ antagonists on cortical and limbic subnetworks, and Bush et al. (1999) found in cortical simulations employing more detailed cell models than ours that $GABA_B$ inhibition was the primary agent in ending epileptic activity. The second and third findings on the dependencies of wave propagation characeristics could be tested by comparison between experiments in cortical areas with differing connectivity structures (see Discussion).

FIGURE 9 ABOUT HERE

Experimental Results on Vertical Transfer

The experiments we have been discussing in relation to horizontal activity spread (Chagnac-Amitai & Connors, 1989a,b; Langdon & Sur (1990) were conducted in rat neocortical slices with direct stimulation just in the lower layers, and therefore provided data on the vertical transfer of activity between cortical layers. Their findings in this regard were:

CC4 Intracellularly recorded superficial pyramidal cells were dominated by IPSPs during wavefront passage, and rarely fired. Deep layer intrinsic bursting cells on the other hand received greater excitation and usually fired; deep regular spiking cells were variable in this respect.

LS4 Local field potentials recorded at sites displaced horizontally from the stimulation point showed that initiation of activity in the deep cortical layers often preceded that in the superficial layers by several milliseconds, suggesting a greater propagation speed in the deep layers.

3-Layer Model: Stimulation and Observed Activity Regimes

Stimulation in the 3-layer model affected the same overall numbers of excitatory and inhibitory cells as previously but was spread across all the layers. To replicate the conditions in Chagnac-Amitai & Connors (1989a,b) in which stimulation was applied within layer VI, excitatory and inhibitory cells were stimulated over a given radius in the deep layers and excitatory cells as well as inhibitory cells with vertical arbors extending into the deep layer were stimulated over a narrower radius in the superficial layer.

Langdon & Sur stimulated the white matter below layer VI in their slices. Though often treated as similar to sensory stimulation, this also activates deep and superficial layer cells via antidromic spiking in addition to orthodromically activating the middle layer (Kenan-Vaknin & Telyer, 1994). Also, the deep layer is more strongly activated than the superficial layer, probably as a result of direct current spread. To replicate Langdon & Sur's conditions, we applied the same stimulation as above except that inhibitory cells were not directly stimulated outside of the middle layer, since they would not have been activated antidromically. (Note that inhibitory cells might be activated disynaptically through the pyramidal cells.)

The 3-layer model displayed the same three regimes of quiescence, wave propagation, and explosion as the 1-layer model, and wave propagation again required $GABA_B$. The main difference was the surprising observation that activity level and propagation speed could differ from layer to layer within the same simulation. Speeds generally differed by 20% or less, but in some cases cells in one layer could be highly active yet completely inactive on another. This was particularly the case at disinhibition levels in which a

wave would propagate for some distance and then die out – activity could persist for as much as 20 msec longer on some layers than on others. We describe this aspect of the results first, then focus on the further activity difference that sometimes occurred between bursting and regular spiking cells in the model's deep layer, analogously to the experimental results reported above.

Comparison of 3-Layer Model with Experiment

Activity Differences Between Layers

Aspects of both the main experimental results on vertical transfer (CC4 and LS4) were demonstrated by the 3-layer model network (Figure 10). Activity levels were highest (highest firing rates, thicker waves, and/or longest active) on the deep layer, lowest on the superficial layer, and intermediate in the middle layer (CC4). Propagation rates were slowest on the superficial layer, 10-15% faster on the middle layer, and 15-25% faster on the deep layer (LS4).

FIGURE 10 ABOUT HERE

We hypothesized that the greater activity in the deep layer was a consequence of the connectional compartmentalization between pyramidal neurons in different layers described in the Methods (65% of connections on average stay within the superficial, middle, or deep compartments). Because the deep layer was stimulated to a wider radius and contained bursting cells (see below), activity started out and remained stronger there than in the other layers. This would imply that the middle layer was more active than the superficial layer for two reasons. First, because the principal output from the deep layer (outside of itself) is to the middle layer, activity was boosted somewhat there as well. Second, the intrinsic excitatory connections in the middle layer arborize over a narrower radius than those in either the deep or superficial layers, which was reported above to contribute to greater intrinsic excitability.

The propagation rate differences observed were likely a consequence of the differences in activity levels: as shown above, high activation is associated with faster propagation, as shown in Figure 8B. However, from the data in this same figure one might expect propagation to be slowest in the narrowly-connected middle layer, despite the greater activity level, since even the fastest propagation for the 'short' condition is slower than the slowest for the 'baseline' condition.

To test our hypothesis and better understand the effects of the moderately weak coupling between layers, two versions of the model were constructed that varied excitatory and inhibitory coupling. In the first version, excitatory connections were made evenly within and between layers – the output axons from every pyramidal cell arborized in all three layers in proportions equal to the proportions of the total pyramidal population in them. When this version was run, both the level of activity and propagation rate were consistently the same in all layers over a range of disinhibition levels (Figures 11, 12) – approximately equal to that for the deep layer in the realistically-connected model. In the second version, excitatory connections were left as is, but all inhibitory connections between layers (27% of all inhibition) were removed and replaced with equivalent within-layer connections. In this model, activity differences between the layers

were sharply reduced (Figure 11). Thus, inhibitory coupling, which allows strong activation in one layer to suppress cells in the other two, plays an important role in allowing activity differences between layers to emerge.

FIGURE 11 ABOUT HERE

FIGURE 12 ABOUT HERE

Activity Differences Between Bursting and Regular Spiking Cells

Chagnac-Amitai & Connors (1989b) reported that bursting cells were consistently about 3 times as active as other pyramidal cells in the deep layers. They postulated that bursting cells might interconnect more densely with each other than with regular spiking cells so that, within this subnetwork, calcium-current-driven excitation could build to high levels. In a few of our simulations, the bursting cells in the deep layer were indeed slightly more highly activated on average than the deep regular spiking cells, however this was not consistent. Increased spiking was presumably due to the presence of the extra depolarizing calcium current that causes bursting behavior, and occurred in the 1-layer simulations as well when a small percentage of bursting cells was included. However any increased activity of bursting cells is translated into synaptic input to other pyramidal cells, particularly those in the deep layer since nearly 80% of the output of deep pyramidal cells remains there. Some increased deep layer activity is also transmitted to the upper layers, however, and in all cases the presence of bursting cells made the networks (both single- and multiple-layer) more excitable, so that the transitions between regimes were shifted towards lower levels of disinhibition.

We examined the causes of the discrepancy between the observations in Chagnac-Amitai & Connors (1989a,b) and our simulations by directly testing their hypothesis that burst cells interconnect more strongly with each other than with regular spiking cells. We constructed a version of the model in which bursting cells made 50–100% of their outgoing pyramidal connections to other bursting cells (in the Baseline version of the model this value was 20%, since this was the proportion they made up of the deep pyramidal population). We found that consistent, strong activity differences emerged at around 70% interconnectivity, and around 90% was sufficient to produce the experimentally observed 3-fold difference in activity level (data not shown). This lends support to the subnetwork hypothesis and suggests that some of our assumptions of minimal complexity in determining cortical connectivity are not always valid. None the less, our primary findings are robust to any reasonable alterations to connectivity, as shown presently.

Effects of Other Parameter Variations in 3-Layer Model

Although the 3-layer model contains many parameters, only a few of these are directly relevant to the result of partial functional isolation between layers. The investigation of the 1-layer model revealed the

dependence of horizontal propagation properties on within-layer connection characteristics. In this section, we address the relation between vertical connectivity and vertical transmission in the 3-layer model, with an eye towards assessing the robustness of our functional isolation result in more detail than just done previously.

The two main classes of parameters are those governing between-layer excitatory and between-layer inhibitory connections. Regarding excitation, we reported already that the strength of the between-layer excitatory connections affects the degree of functional isolation reflected in activity differences. However, results from the 1-layer model demonstrated that for a given number of connections, a more narrowly focused arbor is likely to be more effective in keeping activity on different layers at similar levels. As can be seen from Figure 3 and Table 7, the outgoing connections from the deep layer are already narrow, and therefore relatively effective, while the only wide inter-compartment connection is from superficial to deep; narrowing this last one or widening the deep layer output would be expected to increase the observed activity difference. In simulations of the 3-layer model in which we halved the radius of the superficial→deep connection and doubled the radii of the deep→middle,superficial connections, this is in fact what we found.

Regarding inhibition, we investigated the effects of weakening or strengthening all between-layer inhibitory connections simultaneously, adjusting all within-layer connection strengths in compensation. We found that increasing inhibitory coupling to a point where only 50% of inhibition was received within-layer (ordinarily it was 73%) had little effect on the activity differences between layers but that reducing it to 0 (100% within-layer) had the effect of reducing pyramidal activity differences, as described above in connection with Figure 11, bottom.

In general, connection lengths are quite reliably known from the anatomical data, whereas strengths are more subject to doubt (see Methods). Available evidence has tended to suggest that incoming feedforward synapses to layer IV and those from there to superficial layers are stronger than those between deep and superficial layers (e.g., Callaway (1998); Crick & Koch (1998); Stratford et al. (1996)). In simulations incorporating these biases into our model (we doubled the strength of initial input to the middle layer and the middle→superficial connections, and halved those of the deep→middle,superficial connections), the activity differences between levels were not strongly affected. Essentially, the two sets of changes had opposing effects. Relative to the baseline situation, the middle layer was more strongly activated by orthodromic axons but more weakly activated by the connection from the deep layer, and the superficial layer was more strongly activated by the middle layer but more weakly by the deep.

In conclusion, although radical alterations to our basic interlaminar connectivity scheme may affect our finding of functional isolation between cortical layers, more realistic alterations based on existing evidence will probably not.

Comparison with Optical Recording Results

Optical recording using voltage-sensitive dyes (Grinvald et al., 1988) offers an alternative source of high bandwidth spatiotemporal data on cortical activity spread to the systematic field potential recording studies we focused on above. Here we compare our findings with some of the available optical data.

Tanifuji et al. (1994, 1996) recorded from rat area 17 slices under non-disinhibited conditions with white matter stimulation. They found that activity propagated horizontally over distances up to 1 mm in superficial and deep layers, with an absence of significant activity in layer IV, while under mild disinhibition, propagation would extend to 2 or more mm. In their figures, deep activity often appears to lead that in superficial layers, and they report higher propagation speeds in the deeper layers. Aside from layer IV, these findings are in agreement with both our model's behavior and the earlier-discussed experimental results. Langdon & Sur also found relatively low activity in layer IV (Chagnac-Amitai & Connors did not record there), while activity in the 3-layer model's middle layer was generally quite high.

This discrepancy may be an artifact of ambiguity in the optical and local field potential signals – the more compact geometry of spiny stellate cells relative to pyramidal cells in the vertical direction or cancelling effects from current sources/sinks in other layers could cause the absence of a signal when cells were in fact depolarized and firing. But it is also possible that something in the circuitry of the model differs from the cortex – perhaps recurrent inhibitory synapses are stronger or excitatory ones weaker in layer IV than in other layers, for example (Kyriazi et al., 1998), or the layer VI-layer IV connections preferentially contact inhibitory cells. These possibilities require further investigation.

Nelson and Katz (1995), recording from ferret area 17 slices, found qualitatively similar results to Tanifuji, including relatively high deep layer activity and low layer IV activity relative to that in superficial layers. However, the two groups found divergent propagation speeds (about 60 μm and 160 μm per msec respectively), both different from those in the local field potential recordings we focused on (100 μm/msec). Neither reports precisely how they measured the speeds, and it is uncertain what the source of the discrepancy is.

Finally, both groups examined the effects of vertical cuts through either superficial or deep layers on horizontal propagation, finding that activity could spread through horizontal connections at either depth and regenerate at all levels past the cut via vertical connections. Although we found in the model that, as mentioned, *spiking activity* did not always transmit between layers, membrane potentials were often affected, reflecting synaptic activity which could generate an optical signal like that observed experimentally.

In sum, the available fast optical recording data largely supports the earlier experimental results and our interpretation of them based on the model behavior.

DISCUSSION

Horizontal Connectivity

The comparison of the characteristics of horizontal activity propagation in the model with experiment showed that: 1) a sizable wave regime required $GABA_B$ inhibition, and, 2) the transmission characteris-

tics depended strongly on connection lengths and weakly on synaptic strengths. Both of these findings are at variance with some previous cortical models. Wilson & Cowan (1973) found wave propagation with only a $GABA_A$-like inhibition, while Golomb & Amitai (1997) found that a K^+ current contributing to spike rate adaptation (also included in our model) sufficed in their excitatory-only system. In the latter model, propagation speed depended as strongly on synaptic strength as on length (see also Ermentrout, 1998). The primary reason for both discrepancies is likely the fact that the previous models are 1-dimensional in structure, whereas ours is 2-dimensional (with a limited third dimension). In the 2-dimensional situation, the number of cells recruited into the initial expanding wavefront (and hence the local drive received by cells) scales with the square of the spread radius, whereas in the 1-dimensional models it scales only linearly, providing a possible reason for why explosion is observed in the former where waves are observed in the latter. Although the inhibitory drive also scales with the square, the transient difference between excitation and inhibition – which must exist for propagation – is still of second order. This likely leads to a different dynamics and makes activity quashing more difficult in the 2-dimensional situation.

Previously, at least two modes of wave propagation have been discovered in 1-dimensional systems (Ermentrout, 1998; Golomb et al., 1996; Zhang, 1996) – 'lurching' and 'smooth' modes, the former approximately an order of magnitude slower in speed. We did find a lurching-type propagation within a very restricted parameter range in our $GABA_A$-only network, and the speed was 30% of that in the $GABA_B$ wave mode. We also performed a small number of simulations of a 1-dimensional version of our 1-layer network and found that a smooth, rapid-propagation wave regime with only $GABA_A$ inhibition was easy to obtain, and the speed depended strongly on synaptic strength – supporting the idea that dimensionality of the system is the cause of the discrepancy with earlier models. Although it is beyond the scope of this paper, the interaction of dimensionality with the relative effects of hyperpolarizing and shunting-type inhibition requires further study. (Experimental results in Golomb & Amitai (1997) supporting a strong synaptic strength dependence in a 2-dimensional slice employed high bicuculline concentrations that probably generate a different regime (explosion; Chagnac-Amitai & Connors, 1989a)).

Our findings also demonstrated sensitivity of the dynamical behavior of the network to the shape of the connectivity falloff function. The anatomically realistic composite function provided a better fit to the data than any of the unitary functions. If this structure affects basic parameters of unstructured activity propagation, it may also play a role in more complicated transmissions involved in neural computation. The width of lateral arborization is already known to be of central importance in models of correlation-based Hebbian learning (Goodhill, 1998; Linsker, 1986; Miller et al., 1989; Miller, 1994; Takeuchi & Amari, 1979). Models of development in primary visual cortex typically assume lateral interactions equivalent to the 'short' condition here; our findings recommend exploring the effects of the longer interactions (see Figure 13, left). In fact, recent preliminary modeling work (Goldberg et al., 1999) has shown that longer distance connections can spur the development of orientation maps in absence of visual experience (Crair et al., 1998).

Vertical Connectivity

The experimental finding of greater activity in deep pyramidal cells than superficial (Chagnac-Amitai & Connors, 1989a) seems to be explainable in terms of the combination of greater excitability of bursting cells and strong recurrent connectivity isolating the strongly stimulated deep layer from the others to some extent. When bursting cells were additionally isolated as a subnetwork within this deep layer, their activity was higher than that of the neighboring regular spiking pyramidal cells. The experimental finding of faster propagation in the deep layer appears to relate to this greater activity level; it disappeared when activity levels were equalized in a model network with nonisolating connectivity. Contrary to traditional emphases on vertical connectivity (Mountcastle, 1978, Niebur & Wörgötter, 1994), these findings support a view of the cortex as horizontally integrated and vertically segregated, into two modules.

The contrasting idea of *columnar* modules is largely based on physiological observations that receptive field parameters in sensory areas vary more slowly with vertical distance than horizontal (Hubel & Weisel, 1977; Tanaka, 1996), particularly with regard to position on a map of the receptive surface. We suggest that the latter is to be expected even with the partially decoupled connectivity we emphasize here, since: 1) the *inputs* to an area are organized topographically; 2) connections that do exist between compartments are relatively narrow and would therefore tend to support registration between their representations. With respect to vertical similarities in receptive fields, it should be pointed out that important differences are found as well (e.g., Snodderly & Gur, 1995; Tanaka, 1996). It is also possible that compartmentalization plays an important role in computing different aspects of representations by independent horizontal integrations, which are combined or kept in registration via the weaker connections between compartments (see Callaway (1998) for a related hypothesis).

Anatomically, the idea of vertical modules has arisen from the vertical extension of apical dendrites and the vertical orientation of some of the inhibitory types. However, the first observation is offset by the fact that the most numerous and influential inputs go to the basal dendrites, while the cortical vertical inhibitory cells are not very numerous, particularly in the rat cortex. The interaction between superficial and deep cortical layers is still certainly substantial (particularly when aided by special dendritic amplification mechanisms in some cases (e.g., Larkum et al., 1999; Rhodes & Llinas, 2001)), but our data review and model results suggest that thinking only in terms of horizontally linked columnar modules may ignore an important facet of cortical structure. A better conception is that of two or more vertically opposed sheets exchanging information topographically while integrating it internally over different horizontal domains (see Figure 13, right).

FIGURE 13 ABOUT HERE

Model Construction

Our goal was to lay a better foundation for understanding computation in networks of cortical areas by forming a more rigorous connection between anatomy and model. However, there are many places where

the rigor of our methods can be questioned. In compiling the initial data set from the anatomical literature, we were sometimes forced to make quantitative judgments on the basis of qualitative reports, as, for example, in estimating the percentages of an axonal arbor terminating different cortical layers from a traced picture of the tree. The cell classes we used are not universally agreed upon. The assumptions we made in during constraint satisfaction to fill in missing data oversimplified the situation. There are several reasons we undertook and published our analysis despite these issues.

First, analytical techniques are only going to be improved if analysis is attempted in the first place. With the exception of the work by Braitenberg & Schüz (1991), we are aware of no substantial quantitative analysis of local cortical connectivity at the cell population level. In the case of inter-area connectivity, initial efforts by Maunsell & Van Essen (1983), Rockland & Pandya (1979), and Felleman & Van Essen (1991)) led to more sophisticated work by Young's group (Hilgetag et al., 2000; Young, 1993) and others (e.g., Petroni et al., 2001). We hope this will occur as well here. Two areas where our work could be improved would be to develop a more straightforward, easily-understood method of performing the constraint satisfaction and to explore the sensitivity of the space of solutions to variations in the input parameters in a systematic fashion.

Second, the exercise of attempting to use the largely untapped anatomical data for models can help point out areas where more investigation would be helpful. Again, in the case of inter-areal connectivity, analytical work has been useful in providing a reference to which area-pairs require further investigation, in raising the priority of gathering information on termination and origination layers, and in pointing out the need for greater precision in tracer injections. In the course of the research reported here, we identified the following areas where further anatomical data would be useful.

1. Topping the list is certainly the need for more data on pyramidal cell axon arborizations. These are likely the single most important factor in determining the structure of local cortical interactions. More data on bouton density vs. distance distribution and on the frequency of different cell subcategories needs to be gathered both for well-studied areas such as rat Par1 and macaque V1, and for less studied areas, particularly in the so-called isocortex where gross variability appears to be low but variability in circuit details may not be.

2. The second most important item is likely the need to characterize the source of $GABA_B$ inputs to pyramidal cells. Because this input has a different time course and reversal potential from $GABA_A$ inhibition, it plays a different role than the latter, seen both in our simulation results and the experimental literature, and the range over which its source cells communicate is an important architectural parameter. We narrowed the source down through logical considerations to be either bipolar or ascending/descending cells in the rat, but this needs to be narrowed further and verified observationally.

3. Likewise, more information is needed on the sources of inhibition of inhibition, also a major architectural feature.

4. Finally, more data is needed on the relative frequencies of inhibitory cell types, which itself requires a

greater consensus on cell classification than currently exists. While many anatomists may be reluctant to shoehorn cells into a single classification to fit all needs, modelers need one to do their work.

The third reason for our analysis is that even with its flaws, we believe it produces a more accurate model of cortical circuitry than intuition educated by the anatomical review literature alone. The clearest illustrations of this are our findings that the superficial and infragranular neocortical layers are more strongly connected within themselves than with each other, and that the horizontal connectivity pattern is significantly different from a smooth fall-off with distance. These findings were arrived at through quantitative analysis, yet our simulations show how they might affect theories of function in qualitative ways. Finally, it is worth pointing out that, even if these specific details do not hold up once more data is available or more sophisticated analyses are carried out, they illustrate how quantitative anatomical analysis may play an essential role in developing theories of neocortical function.

Generality of Circuitry

Our methods could be applied to assess the functional correlates of known variations in neocortical architecture between different cortical areas and across species. While that is a subject for a later work, we address the question here of how general the architecture we developed and simulated in this paper is likely to be. Robert (1999) reports on variations in cortical circuitry seen in a comparison of data from 30 areas in the rat, cat, and monkey. Four main points from that work are summarized here.

First, the general inventory of inhibitory celltypes and their arborization characteristics is similar across areas and shows only a few variations across species. In particular, monkeys possess a tall, narrow inhibitory type not clearly found in rats or cats – the *double bouquet cell* (Somogyi & Cowey, 1984), receiving input within superficial layers and sending output to all layers – and they also have a very wide (1 mm or more in diameter) type – the *large basket cell* (Jones & Hendry, 1984) – that is found in intermediate form in cats but not at all in the rat (see Gupta et al. (2000) for a recent, thorough account). These types are both relatively numerous and are likely to affect the form of effective horizontal and vertical interactions.

Second, the characteristics of pyramidal arborizations emphasized earlier (wider and denser within-compartment, width in superficial larger than deep which is in turn larger than middle) appear to be common within the limited data set available (see Methods), but there are prominent exceptions. In particular, deep pyramidal cells in area 17 in cats and monkeys project as strongly to middle and superficial as deep layers. In these cases, local interactions are again likely to be different from those observed in our model.

Third, there are two differences between species across all areas. The first is that the superficial layers become thicker and contain more cells in cats and monkeys relative to rats – comparing rat with monkey agranular areas, where this trend is most pronounced, the rat has 38% of a column's cells in superficial layers, while the monkey has 61%. This trend may be driven by an increased need for interareal connections (implemented mostly by superficial layers) to maintain a given proportion of connectedness in larger brains (Murre & Sturdy, 1995). The second difference is that the proportion of inhibitory cells is increased in the cat and monkey (average 24% in macaque) relative to the rat (average 15.5%).

Fourth, there is one class of areas in all of these species, the agranular areas, for which the structure of

the 3-layer model is not directly applicable, because these areas do not possess a clearly-defined middle layer. Nevertheless, connections to these areas do sometimes terminate preferentially within the middle part of the column (Felleman & Van Essen, 1991), suggesting that the difference may be only the absence of a cell-size difference rather than an alteration in fundamental circuit structure.

Further Reductions in Detail

Even the 3-layer model we developed is still too detailed for many modeling applications. Although simpler cell models such as integrate-and-fire (no leak conductance, bursting, or rate adaptation channels), sigmoid, or linear threshold units could be substituted into the model we presented, this would not satisfy all desire for reduction. For purposes of analytical or computational convenience, or conceptual simplification, many models eliminate inhibitory cell populations or even forgo modeling individual cells at all (e.g., Linsker , 1986; Miller, 1994). In these cases use is often made of *interaction functions* which express the combined effects of excitatory and inhibitory local connections (Wiskott & Sejnowski, 1998) at varying radial distance. Such functions could be derived from the connection structure of the 3-layer model presented here by either summing the efficacies of the various excitatory and inhibitory arbors mediating between the three pyramidal populations in an appropriate way, or by taking spike-triggered correlogram measurements directly from simulations. Although neither approach is without its pitfalls, they offer a rigorous foundation for computational models in the anatomical data that could also be used to test the effects of variations in various biological parameters.

Appendix A: Parameters of Cell Model and Synapses

The parameters for the cells were determined to match input resistances and time constants obtained via physiological measurements (parameters, references, and discussion in Bush & Sejnowski (1993)), according to $g_{leak} = 1/R_{in}$, $C_m = \tau_m/R_m$. Values used were as follows:

Cell Class	g_{leak}	C_m	τ_{refr}
large pyramidal (deep layers)	$2.20 \cdot 10^{-8}$S	$4.44 \cdot 10^{-10}$F	2 msec
small pyramidal (superficial)	$9.09 \cdot 10^{-9}$S	$1.81 \cdot 10^{-10}$F	2 msec
inhibitory	$6.10 \cdot 10^{-9}$S	$9.15 \cdot 10^{-11}$F	1 msec

Descriptions of the implementations of the channels for spike-rate adaptation and bursting in pyramidal cells are given at the end of this appendix. Parameters for excitatory synapses were determined first by setting them to match the somatic effects of alpha function inputs to various locations on the dendrites in the multicompartment NEURON model based on Bush & Sejnowski (1993). The parameters of these initial inputs were set to values (g_{peak}=0.5 nS, τ=1 msec) used by Lytton & Sejnowski, 1991, thought to be roughly accurate of the biological situation.

The excitatory peak conductance values were then scaled to compensate the reduction in total number input to the cell (see Methods), however, the increase was not in direct proportion to the reduction (i.e., factor of 30), because this would have resulted in synapses being too powerful, with only on the order of 2 or 3 activations sufficing to bring a cell to firing threshold. Instead, the synapses were scaled to preserve the variance of input to the cells, assuming a situation in which they receive equal amounts of excitation and inhibition on average. In particular, for a cell receiving n independent inputs each with strength s and firing probability p, let X_E and X_I be binomially distributed random

variables representing numbers of active excitatory and inhibitory synapses at a given time instant so that the input strength is $sX_E - sX_I$:

$$P(X_E = k) = P(X_I = k) = Bin(\frac{n}{2}, k, p) = \left(\begin{array}{c} n/2 \\ k \end{array} \right) p^k (1-p)^{n/2-k}$$

$$\sigma^2(sX_E - sX_I) = E[(sX_E - sX_I)^2] - E^2[sX_E - sX_I] = s^2[E(X_E^2) + E(X_I^2) - 2E(X_E X_I)] - s[E^2(X_E) - E^2(X_I)]$$

$$= s^2[2(\frac{n}{2}p(1-p) + (\frac{n}{2})^2 p^2) - 2(\frac{n}{2})^2 p^2] - 0 = s^2 \cdot n \cdot p(1-p)$$

Here, the second line uses the linearity of expected value, and the third uses well-known properties of the binomial distribution (Papoulis, 1991). Thus, when reducing n by some factor, s should be increased by the square root of the same factor to leave σ^2 unchanged.

Time constants for inhibitory synapses were determined analogously to the excitatory ones, except for those for $GABA_B$ and NMDA, which were set from Benardo (1994) and Jones & Baughman (1988) respectively (note NMDA had a -45mV threshold for activation). However, the peak conductances were not determined directly from the biology, but to balance the overall amount of excitation. (The reason for this was that the biological values are not known precisely, although inhibitory synapses are believed to be stronger than excitatory synapses (e.g., Lytton & Sejnowski, 1991) and they are generally closer to the soma.) This was done by setting the inhibitory g_{peak} so that the net inhibitory potential balanced the net excitatory potential at threshold:

$$g_{exc} n_{exc} (E_{exc} - \theta) = -g_{inh} n_{inh} (E_{inh} - \theta)$$

Here, n represents the number of inputs, g the peak conductance, and E, the weighted average reversal potential. The final parameters (time constant (τ), peak conductance, and reversal potential) are listed below for the classes of synapses employed.

Target Celltype	**Synapse Class**	τ	g_{peak}	**E**
pyramidal	proximal exc. (AMPA)	0.50 msec	7.2 nS	0 mV
	mid exc. (AMPA)	0.80 msec	3.8 nS	0 mV
	distal exc. (AMPA)	0.93 msec	2.9 nS	0 mV
	soma shunt ($GABA_A$)	0.42 msec	33 nS	-75 mV
	proximal shunt ($GABA_A$)	0.50 msec	17 nS	-75 mV
	distal hyperpol. ($GABA_B$)	23 msec	1.5 nS	-90 mV
	exc. (NMDA)	10 msec	0.4-1.5 nS	0 mV
inhibitory	exc. (AMPA)	0.50 msec	7.2 nS	0 mV
	inh. ($GABA_A$)	0.45 msec	33 nS	-75 mV

AHP Channel Implementation

Parameters:	G_{max} (50 nS): maximum conductance of the channel.
	anum (4): number of spikes required to raise conductance to G_{max}.
	atime (100 ms): time required for decay from G_{max} to 0.
State variables:	G_k: present conductance of the channel.
Update Procedure:	On firing, increment G_k by $G_{max}/anum$, with ceiling G_{max}. On nonfiring timesteps, decrement G_k by $G_{max}/atime$, with floor 0.

Burst Channel Implementation

Parameters:	bG_k (8 nS): base amplitude of the conductance pulse. *Bac_thresh* (-45 mV): threshold for activating conductance pulse when channel is in active state. *Bt_inc* (10-30 ms): conductance pulse width. *Binac_thresh* (-45 mV): threshold above which channel inactivates on remaining there for longer than *Binac_time* (10 ms). *Btin_inc* (20 ms): time channel remains inactive subsequent to potential dropping below threshold after inactivation.
State variables:	*burst*: flag whether a conductance pulse (burst) is currently in progress, and *Btime* is how much time remains in it. *B_actstate*: flag whether channel is inactivated, and, if so, *Bintime* is how much inactivation time remains. *Bovertime*: how long cell has been over its inactivation threshold. G_k: present conductance of the channel.
Update Procedure:	If bursting, decrement Btime by value of timestep, and if this reaches 0 set burst to 0 and Bintime to Btin_inc. Otherwise if activated, check against Bac_thresh; if over set Btime to Bt_inc and set burst to 1; otherwise check against Binac_thresh and increment Bovertime if over. If Bovertime exceeds Binac_time, set Bintime to Btin_inc, Bovertime to 0, B_actstate to 0. If inactivated, decrement Bintime, and if reaches 0 set B_actstate to 1. Finally, after this bookkeeping, set conductance to bG_k if bursting, 0 otherwise.

Appendix B: Description of Connectivity Optimization Procedure

As described in the Methods, parameters relating to cell type population densities and contact preferences were tuned by taking account of constraints of two types. The first arises from requiring that, when cell outputs are made according to the current parameter values, the resulting numbers of inputs of each of the various types that cells receive are correct (as given by the current parameter values). In calculating the inputs based on outputs (and this calculation could just as well be done in the opposite direction from input to output), the relative densities of the various cell populations are taken into account, along with their respective axonal and dendritic arborizations (see Tables 2 and 7). The second set of constraints are simply the hard constraints arising from hierarchical relations, such as that the population densities of each of the inhibitory types in a layer sum to the total inhibitory density known for the layer.

These latter type of constraints are represented in the table below, which lists all of the classes of parameters that were adjusted in optimization. Each level of indentation in the left-hand column implies a hard constraint. For example, for the top three rows, the total density for the inhibitory populations in layers I-VI should equal the overall inhibitory density, and the total density for each type (chandelier, basket, etc.) should also sum to this value. We have not explicitly listed *every* parameter optimized, but from the examples given in the right-hand column, the full range of instances should be clear. (Note that celltial stands for 'Celltype In A Layer' (Gremillion, 1993)).

Ref	**Type**	**Example**
D1	supertype density	excitatory, inhibitory
D2	layer density	layer II inhibitory
D3	celltype density	chandelier, basket
D4	celltial density	chandelier layer II, basket layer III
O1	celltial total out	basket layer III out
O2	celltial output type out	basket layer III somatic out

C	celltial-celltial i/o	basket layer III to pyramidal layer III output
I3	celltial total in from type	pyramidal layer III basket somatic input
I2	celltial total in from syn class	pyramidal layer III somatic input
I1	celltial total input	pyramidal layer III total input

For each parameter, an estimate and a confidence value were specified based on the data collected and described in the Methods. Confidence values were set at one of 10 levels between 0 and 1 dependent on the certainty of the value itself or of those its estimate was based on. The arborization parameters (width and percentage of axon or dendrite in each layer for each celltial) were not adjusted during optimization. In words, the algorithm functioned in the following way:

> At each step, all outputs from celltials are calculated according to the density and contact preferences parameters, and the arbors, then the errors are calculated on the input side based on the discrepancies. These errors are weighted by the degree of confidence in the desired input values they were calculated from and propagated back to the outputs. Adjustments are made to both input and output parameters as well as densities with magnitudes proportional to those of the errors, but inversely proportional to the degree of confidence in their original estimates. But since both the inputs and outputs (the parameters immediately above and below celltial-celltial i/o in the table above) are impacted by a number of other parameters hierarchically above them, these parameters must be adjusted as well. This is done by propagating the error through the hierarchy in a similar way to the back-propagation neural network weight update algorithm (Rumelhart et al., 1986).

In more detail, the algorithm functioned as follows:

1. For each output type of each celltial (reference 'O2' in table above), calculate its output to each other input type of each celltial, through the formulas:

$$N_{out} = O2 \cdot \sum_{\text{layers}} \text{axon\_pct} \cdot \text{dest\_share}$$

$$N_{in} = N_{out} \cdot \frac{D4_{src}}{D4_{dst}}$$

   Here, 'N_{out}' and 'N_{in}' refer to the number of output synapses and input synapses per cell in the connection between a single pair of cell populations. The output and input per cell differ based on the difference in density of the two populations. The term 'axon_pct' in the first equation is equal to the percentage of the source celltial's axon arborizing in the layer of contact with the destination celltial's dendrites (see Tables 2, 5, 7). The 'dest_share' parameter is the percentage of the total dendritic surface eligible to receive this type of output the destination celltial's dendrites make up in the layer of contact. The resulting products are summed over all layers of contact. The total output for the type will sum to the desired amount (O2) over all destination celltials.

2. Propagate the input numbers by summation up through 'I3–I1' to the total inputs for each cell. This allows computation of discrepancy (error) at each level. For example, pyramidal cells in all layers receive somatic input from both basket cells and spiderweb cells. For a given layer, the inputs to the pyramidal population deriving from basket cells in all layers that contact them are summed to provide one of the values for I3. This number is summed with the corresponding value for spiderweb cells to produce I2, which can be compared with the anatomically-derived value for number of somatic synapses for pyramidals in this layer. Finally, this would be summed with values for dendritic synapses (both inhibitory and excitatory) to produce a value for I1.

3. Calculate error at I1 by formula:

$$E = C_o \cdot \frac{s - o}{o}$$

   Here, s and o refer to the currently set and original (experimentally estimated) values for an input parameter, while C_o refers to the confidence in the original value. The absolute discrepancy ($s - o$) between the two values is scaled by the original value

to make error a relative measure independent of parameter size, and it is multiplied by the confidence level in the original estimate so that discrepancies from values that are well-established are weighted more heavily. The resulting error value may be positive or negative, and is generally of a magnitude less than 1.

4. The provisional local error at I2 is calculated by the same formula as in I1, except that the 'set' and 'original' values now refer to the summands contributing to the totals at I1. Then this local error is combined with the parent error using the formula:

$$p \cdot E_{\text{parent}} + (1 - p) \cdot E_{\text{local}}$$

Here, 'p' is the percentage the class of input accounted for at I2 makes up of the total input to the celltial at I1. This effectively assigns the parameter a proportion of the responsibility for the parent's error commensurate with its contribution to it, similarly to the back-propagation algorithm, but with the addition of the local error factored in. An analogous process is then carried out at I3, with I2 playing the part of the parent.

5. At this point, the overall error state of the network is measured and used to determine whether to terminate the optimization.

6. The error is transferred over from I3 to O2 through C, computed as the weighted sum from the error over all the connections to other celltials (actually input types (I3) of celltials) that are made. Each weight is equal to the proportion of the output of this type that the celltial/input type receives. Thus, the weight given to the error from connection i is equal to $N_{out_i} / \sum_j N_{out_j}$, where i and the sum range over all of the connections made.

7. The error is propagated from O2 to O1 and then successively up to D4, D3, D2, and D1. At each of the stages O2 to O1, D4 to D3, D4 to D2, and D3 to D1, propagation consists in summing the errors from the "child" parameters, weighted by the proportions they make up of the total. For example, from D4 to D3 for basket cells, the errors for basket cells in each layer are summed, weighted by the proportion they make up of the total basket cell population. The errors at O2 and D4 are each set to half the weighted sum calculated at O2. Because confidence in them is complete, the parameter values at D2 are held fixed, and only the error at D3 determines that at D1. This is done since, in the succeeding step, the D1 value is used as part of the determination for adjustment of D3. Although it would be possible to allow the D2 error to also contribute here, this might lead to instability and failure to converge. The error at D2 does contribute, however, to adjustments at D4.

8. Adjustments based on the errors are performed bottom-up from O2→O1→D4→(D3,D2)→D1, and then multiplicative normalization is performed in the opposite direction, starting from D1. At each stage, the first adjustment is made by:

$$s'_t = s_t + rEs_t + a$$

$$s_{t+1} = s'_t + (o - s'_t) \cdot C_o$$

Here, s_t represents the current setting of the parameter value at step t, o represents the original estimated value, and C the confidence in that value; r is a rate parameter global to the entire optimization and fixed for its duration, and a is a noise value generated separately for each parameter according to the Gaussian distribution $N(0, \sigma \cdot o)$. The variance σ is global to the entire optimization and varied according to an annealing schedule as follows:

$$\sigma = \frac{\text{nsteps} - \text{step}}{\text{nsteps}} \cdot \text{annealMax}$$

The first adjustment equation corrects for the error summed and normalized over all inputs affected by the output this parameter affects, and the second one pulls back towards the estimated value based on confidence level. After such adjustments have been made at all levels of the hierarchy, multiplicative normalization is employed, starting from D1, to enforce hard constraints. For instance, for the relation between D1 and D2, for each D1 type (inhibitory and excitatory), the parameter values D2 are summed over the layers, and then they are all multiplied by a factor to make the sum equal to the D1 value. For example, for the i_{th} D1 parameter value, $D2_{ij} = D2_{ij} / \sum_k D2_{ik} / D1_i$

9. Control is returned to step 1.

The above sequence was applied iteratively, and typically the configuration of input/output and distribution parameters relaxed to a stable state after 10–100 steps depending on the rate parameter.

Acknowledgements

The authors would like to thank Ed Callaway for helpful discussions regarding cortical anatomy. Research supported by the San Diego McDonnell-Pew Center for Cognitive Neuroscience and the UCSD Center for Human Information Processing. Reprint requests to: Martin I. Sereno; Department of Cognitive Science 0515; University of California, San Diego; 9500 Gilman Drive; La Jolla, CA 92093.

References

[1] Amir, Y., Harel, M., and Malach, R. (1993). Cortical hierarchy reflected in the organization of intrinsic connections in macaque monkey visual cortex. *J. Comp. Neurol.*, 334:19–46.

[2] Badran, S., Schmutz, M., and Olpe, H. R. (1997). Comparative in vivo and in vitro studies with the potent GABA-B receptor antagonist, CGP 56999A. *Eur. J. Pharmacol.*, 333:135–42.

[3] Beaulieu, C. (1993). Numerical data on neocortical neurons in adult rat, with special reference to the GABA population. *Brain Res.*, 609:284–92.

[4] Beaulieu, C., Campistron, G., and Crevier, C. (1994). Quantitative aspects of the GABA circuitry in the primary visual cortex of the adult rat. *J. Comp. Neurol.*, 339:559–72.

[5] Benardo, L. S. (1994). Separate activation of fast and slow inhibitory postsynaptic potentials in rat neocortex in vitro. *J. Physiol.*, 476:203–15.

[6] Bernander, O., Koch, C., and Usher, M. (1994). The effects of synchronized inputs at the single neuron level. *Neural Computation*, 6:622–41.

[7] Braitenberg, V. and Schüz, A. (1991). *Anatomy of the Cortex*. Berlin: Springer-Verlag.

[8] Buhl, E., Han, Z., Lorinczi, Z., Stezhka, V., Karnup, S., and Somogyi, P. (1994). Physiological properties of anatomically identified axo-axonic cells in the rat hippocampus. *J. Neurophysiol.*, 71:1289–307.

[9] Bush, P., Prince, D., and Miller, K. (1999). Increased pyramidal excitability and NMDA conductance can explain posttraumatic epileptogenesis without disinhibition: A model. *J. Neurophysiol.*, 82:1748–58.

[10] Bush, P. C. and Sejnowski, T. J. (1993). Reduced compartmental models of neocortical pyramidal cells. *J. Neurosci. Meth.*, 46:159–66.

[11] Bush, P. C. and Sejnowski, T. J. (1994). Effects of inhibition and dendritic saturation in simulated neocortical pyramidal cells. *J. Neurophysiol.*, 71:2183–93.

[12] Bush, P. C. and Sejnowski, T. J. (1996). Inhibition synchronizes sparsely connected cortical neurons within and between columns in realistic network models. *J. Comput. Neurosci.*, 3:91–110.

[13] Caddick, S. J. and Hosford, D. A. (1996). The role of GABA-B mechanisms in animal models of absence seizures. *Molec. Neurobiol.*, 13:23–32.

[14] Callaway, E. M. (1998). Local circuits in primary visual cortex of the macaque monkey. *Annu. Rev. Neurosci.*, 21:47–74.

[15] Callaway, E. M. and Wiser, A. K. (1996). Contributions of individual layer 2-5 spiny neurons to local circuits in macaque primary visual cortex. *Vis. Neurosci.*, 13:907–22.

[16] Chagnac-Amitai, Y. and Connors, B. W. (1989a). Horizontal spread of synchronized activity in neocortex and its control by GABA-mediated inhibition. *J. Neurophysiol.*, 61:747–58.

[17] Chagnac-Amitai, Y. and Connors, B. W. (1989b). Synchronized excitation and inhibition driven by intrinsically bursting neurons in neocortex. *J. Neurophysiol.*, 62:1149–62.

[18] Conde, F., Lund, J. S., Jacobowitz, D. M., Baimbridge, K. G., and Lewis, D. A. (1994). Local circuit neurons immunoreactive for calretinin, calbindin D-28k, or parvalbumin in monkey prefrontal cortex: Distribution and morphology. *J. Comp. Neurol.*, 341:95–116.

[19] Connors, B., Malenka, R., and Silva, L. (1988). Two inhibitory postsynaptic potentials, and GABAA and GABAB receptor-mediated responses in neocortex of rat and cat. *J. Physiol.*, 406:443–68.

[20] Connors, B. W., Gutnick, M. J., and Prince, D. A. (1982). Electrophysiological properties of neocortical neurons in vitro. *J. Neurophysiol.*, 48:1302–20.

[21] Crair, M. C., Gillespie, D. C., and Stryker, M. P. (1998). The role of visual experience in the development of columns in cat visual cortex. *Science*, 279:566–9.

[22] Crick, F. and Koch, C. (1998). Constraints on cortical and thalamic projections: The no-strong-loops hypothesis. *Nature*, 391:245–50.

[23] de Lima, A. D. and Morrison, J. H. (1989). Ultrastructural analysis of somatostatin-immunoreactive neurons and synapses in the temporal and occipital cortex of the macaque monkey. *J. Comp. Neurol.*, 283:212–27.

[24] DeFelipe, J. and Farinas, I. (1992). The pyramidal neuron of the cerebral cortex: Morphological and chemical characteristics of the synaptic inputs. *Progr. Neurobiol.*, 39:563–607.

[25] DeFelipe, J., Hendry, S. H., and Jones, E. G. (1986). A correlative electron microscopic study of basket cells and large GABAergic neurons in the monkey sensory-motor cortex. *Neurosci.*, 17:991–1009.

[26] DeFelipe, J., Hendry, S. H., and Jones, E. G. (1989). Visualization of chandelier cell axons by parvalbumin immunoreactivity in monkey cerebral cortex. *Proc. Natl. Acad. Sci. USA*, 86:2093–7.

[27] DeFelipe, J., Hendry, S. H., Jones, E. G., and Schmechel, D. (1985). Variability in the terminations of GABAergic chandelier cell axons on initial segments of pyramidal cell axons in the monkey sensory-motor cortex. *J. Comp. Neurol.*, 231:364–84.

[28] Del Rio, M. R. and DeFelipe, J. (1994). A study of SMI 32-stained pyramidal cells, parvalbumin-immunoreactive chandelier cells, and presumptive thalamocortical axons in the human temporal neocortex. *J. Comp. Neurol.*, 342:389–408.

[29] Douglas, R. and Martin, K. (1991). A functional microcircuit for cat visual cortex. *J. Physiol.*, 440:735–69.

[30] Douglas, R. J., Koch, C., Mahowald, M., Martin, K. A. C., and Suarez, H. H. (1995). Recurrent excitation in neocortical circuits. *Science*, 269:981–5.

[31] Douglas, R. J., Martin, K. A. C., and Whitteridge, D. (1989). A canonical circuit for neocortex. *Neural Computation*, 1:480–8.

[32] Eder, M., Rammes, G., Zieglgansberger, W., and Dodt, H. (2001). GABA(A) and GABA(B) receptors on neocortical neurons are differentially distributed. *Eur. J. Neurosci.*, 13:1065–9.

[33] Elston, G., Pow, D., and Calford, M. (1997). Neuronal composition and morphology in layer IV of two vibrissal barrel subfields of rat cortex. *Cerebral Cortex*, 7:422–31.

[34] Ermentrout, B. (1998). The analysis of synaptically generated traveling waves. *J. Comput. Neurosci.*, 5:191–208.

[35] Erwin, E., Obermayer, K., and Schulten, K. (1995). Models of orientation and ocular dominance columns in the visual cortex: A critical comparison. *Neural Computation*, 7:425–68.

[36] Felleman, D. J. and Van Essen, D. C. (1991). Distributed hierarchical processing in the primate cerebral cortex. *Cerebral Cortex*, 1:1–47.

[37] Fonseca, M., Soriano, E., I., F., Martinez, A., and Tunon, T. (1993). Chandelier cell axons identified by parvalbumin-immunoreactivity in the normal human temporal cortex and in Alzheimer's disease. *Neurosci.*, 55:1107–16.

[38] Fuentes, U., Ritz, R., Gerstner, W., and van Hemman, J. L. (1996). Vertical signal flow and oscillations in a three-layer model of the cortex. *J. Comput. Neurosci.*, 3:125–36.

[39] Gabbott, P. L. and Bacon, S. J. (1996). Local circuit neurons in the medial prefrontal cortex (areas 24a,b,c, 25, and 32) in the monkey: II. Quantitative areal and laminar distributions. *J. Comp. Neurol.*, 364:609–36.

[40] Gabbott, P. L., Dickie, B. G., Vaid, R. R., Headlam, A. J., and Bacon, S. J. (1997). Local-circuit neurones in the medial prefrontal cortex (areas 25, 32, and 24b) in the rat: Morphology and quantitative distribution. *J. Comp. Neurol.*, 377:465–99.

[41] Ghosh, S. and Porter, R. (1988). Morphology of pyramidal neurones in monkey motor cortex and the synaptic actions of their intracortical axon collaterals. *J. Physiol.*, 400:593–615.

[42] Goldberg, D. H., Shouval, H., and Cooper, L. N. (1999). Lateral connectivity as a scaffold for developing orientation preference maps. *Neurocomputing*, to appear.

[43] Golomb, D. and Amitai, Y. (1997). Propagating neuronal discharges in neocortical slices: Computational and experimental study. *J. Neurophysiol.*, 78:1199–1211.

[44] Golomb, D., Wang, X., and Rinzel, J. (1996). Propagation of spindle waves in a thalamic slice model. *J. Neurophysiol.*, 75:750–69.

[45] Gonchar, Y. and Burkhalter, A. (1999). Connectivity of GABAergic calretinin-immunoreactive neurons in rat primary visual cortex. *Cereb. Cortex*, 9:683–96.

[46] Goodhill, G. J. (1998). The influence of neural activity and intracortical connections on the periodicity of ocular dominance stripes. *Network*, 9:419–32.

[47] Gottlieb, J. P. and Keller, A. (1997). Intrinsic circuitry and physiological properties of pyramidal neurons in rat barrel cortex. *Exper. Brain Res.*, 115:47–60.

[48] Gremillion, M. A. V. (1993). *Modeling Receptive Field Properties of Cat Visual Pathway Neurons Through Spatial Population Interactions*. PhD thesis, Department of Biology, UCSD.

[49] Grinvald, A., Frostig, R. D., Lieke, E., and Hildesheim, R. (1988). Optical imaging of neuronal activity. *Physiol. Rev.*, 68:1285–1366.

[50] Gupta, A., Wang, Y., and Markram, H. (2000). Organizing principles for a diversity of gabaergic interneurons and synapses in the neocortex. *Science*, 287:273–8.

[51] Hellwig, B., Schüz, A., and Aertsen, A. (1994). Synapses on axon collaterals of pyramidal cells are spaced at random intervals: A golgi study in the mouse cerebral cortex. *Biol. Cybern.*, 71:1–12.

[52] Hilgetag, C. C., O'Neill, M. A., and Young, M. P. (2000). Hierarchical organization of the macaque and cat cortical sensory systems explored with a novel network processor. *Phil. Trans. Roy. Soc. London B*, 355:71–89.

[53] Hines, M. L. and Carnevale, N. T. (1997). The NEURON simulation environment. *Neural Computation*, 9:1179–209.

[54] Hubel, D. H. and Wiesel, T. N. (1977). Functional architecture of macaque monkey visual cortex. *Proc. R. Soc. London Ser. B*, 198:1–59.

[55] Hubener, M., Schwarz, C., and Bolz, J. (1990). Morphological types of projection neurons in layer 5 of cat visual cortex. *J. Comp. Neurol.*, 301:655–74.

[56] Hwa, G. G. and Avoli, M. (1991). The involvement of excitatory amino acids in neocortical epileptogenesis: NMDA and non-NMDA receptors. *Exp. Brain Res.*, 86:248–56.

[57] Jack, J., Noble, A., and Tsien, R. W. (1975). *Electric Current Flow in Excitable Cells*. Oxford: Clarendon Press.

[58] Johnson, R. R. and Burkhalter, A. (1996). Microcircuitry of forward and feedback connections within rat visual cortex. *J. Comp. Neurol.*, 368:383–98.

[59] Jones, E. G. (1984). Neurogliaform, or spiderweb cells. In Jones, E. G. and Peters, A., editors, *Cerebral Cortex, Volume I: Cellular Components of the Cerebral Cortex*. New York: Plenum.

[60] Jones, E. G. and Hendry, S. H. (1984). Basket cells. In Jones, E. G. and Peters, A., editors, *Cerebral Cortex, Volume I: Cellular Components of the Cerebral Cortex*. New York: Plenum.

[61] Jones, E. G., Hendry, S. H., and DeFelipe, J. (1987). GABA-peptide neurons of the primate cerebral cortex: A limited cell class? In Jones, E. G. and Peters, A., editors, *Cerebral Cortex, Volume VI: Further Aspects of Cortical Function, Including Hippocampus*. New York: Plenum.

[62] Jones, E. G. and Peters, A., editors (1984). *Cerebral Cortex, Vol. I. Cellular Components of the Cerebral Cortex*. New York: Plenum.

[63] Jones, K. A. and Baughman, R. W. (1988). NMDA and non-NMDA-receptor components of excitatory synaptic potentials recorded from cells in layer V of rat visual cortex. *J. Neurosci.*, 8:3522–34.

[64] Kang, Y. and Kayano, F. (1994). Electrophysiological and morphological characteristics of layer VI pyramidal cells in the cat motor cortex. *J. Neurophysiol.*, 72:578–91.

[65] Karlsson, G., Kolb, C., Hausdorf, A., Portet, C., Schmutz, M., and Olpe, H. (1992). GABA-B receptors in various in vitro and in vivo models of epilepsyl a study with the GABA-B receptor blocker CGP 35348. *Neurosci.*, 47:63–8.

[66] Karlsson, G. and Olpe, H. R. (1989). Inhibitory processes in normal and epileptic-like rat hippocampal slices: The role of GABA-B receptors. *Eur. J. Pharmacol.*, 163:285–90.

[67] Keller, A. and Asanuma, H. (1993). Synaptic relationships involving local axon collaterals of pyramidal neurons in the cat motor cortex. *J. Comp. Neurol.*, 336:229–242.

[68] Kenan-Vaknin, G. and Teyler, T. J. (1994). Laminar pattern of synaptic activity in rat primary visual cortex: Comparison of in vivo and in vitro studies employing the current source density analysis. *Brain Res.*, 635:37–48.

[69] Kisvarday, Z. F., Beaulieu, C., and T., E. U. (1993). Network of GABAergic large basket cells in cat visual cortex (area 18): Implication for lateral disinhibition. *J. Comp. Neurol.*, 327:398–415.

[70] Kisvarday, Z. F. and Eysel, U. T. (1993). Functional and structural topography of horizontal inhibitory connections in cat visual cortex. *Eur. J. Neurosci.*, 5:1558–72.

[71] Kisvarday, Z. F., Gulyas, A., Beroukas, D., North, J. B., Chubb, I. W., and Somogyi, P. (1990). Synapses, axonal and dendritic patterns of GABA-immunoreactive neurons in human cerebral cortex. *Brain*, 113:793–812.

[72] Kyriazi, H., Carvell, G. E., Brumberg, J. C., and Simons, D. J. (1998). Laminar differences in bicuculline methiodide's effects on cortical neurons in the rat whisker/barrel system. *Somatosensory and Motor Research*, 15:146–56.

[73] Langdon, R. B. and Sur, M. (1990). Components of field potentials evoked by white matter stimulation in isolated slices of primary visual cortex: Spatial distributions and synaptic order. *J. Neurophysiol.*, 64:1484–1501.

[74] Larkman, A. U. (1991). Dendritic morphology of pyramidal neurones of the visual cortex of the rat. III. Spine distributions. *J. Comp. Neurol.*, 306:332–43.

[75] Larkum, M. E., Zhu, J. J., and Sakmann, B. (1999). A new cellular mechanism for coupling inputs arriving at different cortical layers. *Nature*, 398:338–41.

[76] Levitt, J. B., Lewis, D. A., Yoshioka, T., and Lund, J. S. (1993). Topography of pyramidal neuron intrinsic connections in macaque monkey prefrontal cortex (areas 9 and 46). *J. Comp. Neurol.*, 338:360–76.

[77] Lewis, D. and Lund, J. (1990). Heterogeneity of chandelier neurons in monkey neocortex: Corticotropin releasing factor and parvalbumin-immunoreactive populations. *J. Comp. Neurol.*, 293:599–615.

[78] Linsker, R. (1986). From basic network principles to neural architecture: Emergence of orientation columns. *Proc. Natl. Acad. Sci. U. S. A.*, 83:8779–83.

[79] Lubke, J., Egger, V., B., S., and Feldmeyer, D. (2000). Columnar organization of dendrites and axons of single and synaptically coupled excitatory spiny neurons in layer IV of the rat barrel cortex. *J. Neurosci*, .20:5300–11.

[80] Lumer, E. D., Edelman, G. M., and Tononi, G. (1997). Neural dynamics in a model of the thalamocortical system: I. Layers, loops, and the emergence of fast synchronous synchronous rhythms. *Cerebral Cortex*, 7:207–27.

[81] Lund, J. S. and Lewis, D. A. (1993). Local circuit neurons of developing and mature macaque prefrontal cortex: Golgi and immunocytochemical characteristics. *J. Comp. Neurol.*, 328:282–312.

[82] Lytton, W. and Sejnowski, T. J. (1991). Simulations of cortical pyramidal neurons synchronized by inhibitory interneurons. *J. Neurophys.*, 66:1059–79.

[83] Marin-Padilla, M. (1984). Neurons of layer I: A developmental analysis. In Jones, E. G. and Peters, A., editors, *Cerebral Cortex, Volume I: Cellular Components of the Cerebral Cortex*. New York: Plenum.

[84] Marin-Padilla, M. (1987). The chandelier cell of the human visual cortex: A golgi study. *J. Comp. Neurol.*, 265:61–70.

[85] Marin-Padilla, M. (1990a). The pyramidal cell and its local-circuit interneurons: A hypothetical unit of the mammalian cerebral cortex. *J. Cog. Neurosci.*, 2:180–194.

[86] Marin-Padilla, M. (1990b). Three-dimensional structural organization of layer I of the human cerebral cortex: A Golgi study. *J. Comp. Neurol.*, 299:89–105.

[87] Martin, K. A., Friedlander, M. J., and Alones, V. (1989). Physiological, morphological, and cytochemical characteristics of a layer I neuron in cat striate cortex. *J. Comp. Neurol.*, 282:404–14.

[88] Martin, K. A. and Whitteridge, D. (1984). Form, function, and intracortical projections of spiny neurones in the striate visual cortex of the cat. *J. Physiol.*, 353:463–504.

[89] Martin, K. A. C., Somogyi, P., and Whitteridge, D. (1983). Physiological and morphological properties of identified basket cells in the cat's visual cortex. *Exp. Brain Res.*, 50:193–200.

[90] Maunsell, J. H. and Van Essen, D. C. (1983). The connections of the middle temporal visual area (MT) and their relationship to a cortical hierarchy in the macaque monkey. *J. Neurosci.*, 3:2563–86.

[91] McCormick, D. A., Connors, R. W., Lighthall, J. W., and Prince, D. A. (1985). Comparative electrophysiology of pyramidal and sparsely spiny stellate neurons of the neocortex. *J. Neurophysiol.*, 59:782–806.

[92] Meskenaite, V. (1997). Calretinin-immunoreactive local circuit neurons in area 17 if the cynomolgus monkey, macaca fascicularis. *J. Comp. Neurol.*, 379:113–32.

[93] Miller, K. D. (1994). A model for the development of simple cell receptive fields and the ordered arrangement of orientation columns through activity-dependent competition between ON and OFF-center inputs. *J. Neurosci.*, 14:409–41.

[94] Miller, K. D., Keller, J. B., and Stryker, M. P. (1989). Ocular dominance column development: Analysis and simulation. *Science*, 245:605–15.

[95] Mitzdorf, U. (1985). Current source-density method and application in cat cerebral cortex: Investigation of evoked potentials and EEG phenomena. *Physiol. Rev.*, 65:37–100.

[96] Mountcastle, V. (1978). An organizing principle for cerebral function: The unit module and the distributed system. In Edelman, G. M. and Mountcastle, V. B., editors, *The Mindful Brain*. Cambridge, Mass.: MIT Press.

[97] Murre, J. M. and Sturdy, D. P. (1995). The connectivity of the brain: Multi-level quantitative analysis. *Biological Cybernetics*, 73:529–45.

[98] Neibur, E. and Wörgötter, F. (1994). Design principles of columnar organization in visual cortex. *Neural Computation*, 6:602–14.

[99] Nelson, D. A. and Katz, L. C. (1995). Emergence of functional circuits in ferret visual cortex visualized by optical imaging. *Neuron*, 15:23–34.

[100] Ojima, H., Honda, C. N., and Jones, E. G. (1991). Patterns of axon collateralization of identified supragranular pyramidal neurons in the cat auditory cortex. *Cerebral Cortex*, 1:80–94.

[101] Ojima, H., Honda, C. N., and Jones, E. G. (1992). Characteristics of intracellularly injected infragranular pyramidal neurons in cat primary auditory cortex. *Cerebral Cortex*, 2:197–216.

[102] Ong, J. and Kerr, D. I. (1994). Suppression of GABA-B receptor function in rat neocortical slices by amiloride. *Eur. J. Pharmacol.*, 260:73–7.

[103] Paldino, A. M. and Harth, E. (1977). Some quantitative results on golgi impregnated axons in rat visual cortex using a computer assisted video digitizer. *J. Comp. Neurol.*, 176:247–62.

[104] Papoulis, A. (1991). *Probability, Random Variables, and Stochastic Processes*. New York: McGraw-Hill.

[105] Patton, P., Thomas, E., and Wyatt, R. E. (1992). A computational model of vertical signal propagation in the primary visual cortex. *Biol. Cybern.*, 68:43–52.

[106] Peters, A. (1984). Chandelier cells. In Jones, E. G. and Peters, A., editors, *Cerebral Cortex, Volume I: Cellular Components of the Cerebral Cortex*. New York: Plenum.

[107] Peters, A. and Harriman, K. M. (1988). Enigmatic bipolar cell of rat visual cortex. *J. Comp. Neurol.*, 267:409–32.

[108] Peters, A. and Harriman, K. M. (1992). Different kinds of axon terminals forming symmetric synapses with the cell bodies and initial axon segments of layer II/III pyramidal cells. *J. Neurocyt.*, 21:679–92.

[109] Petroni, F., Panzeri, S., Hilgetag, C., Kotter, R., and Young, M. (2001). Simultaneity of responses in a hierarchical visual network. *Neuroreport*, 12:2753–9.

[110] Press, W. H., Teukolsky, S. A., Vetterling, W. T., and Flannery, B. P. (1992). *Numerical Recipes in C, Second Edition*. Cambridge: Cambridge University Press.

[111] Prieto, J. J., Peterson, B. A., and Winer, J. A. (1994). Morphology and spatial distribution of GABAergic neurons in cat primary auditory cortex (AI). *J. Comp. Neurol.*, 344:349–82.

[112] Prince, D. A. and Huguenard, J. R. (1988). Functional properties of neocortical neurons. In P. Rakic, W. S., editor, *Neurobiology of Neocortex*. New York: Wiley.

[113] Rhodes, P. and R.R., L. (2001). Apical tuft input efficacy in layer 5 pyramidal cells from rat visual cortex. *J. Physiol.*, 536:167–87.

[114] Robert, A. (1999). *Lamination and Within-Area Integration in the Neocortex*. PhD thesis, Department of Cognitive Science, University of California at San Diego.

[115] Rockland, K. S. and Pandya, D. N. (1979). Laminar origins and terminations of cortical connections of the occipital lobe in the rhesus monkey. *Brain Res.*, 179:3–20.

[116] Rumelhart, D. E., Hinton, G. E., and Williams, R. J. (1986). Learning internal representations by error propagation. In Rumelhart, D. E., McClelland, J. L., and Group, T. P. R., editors, *Parallel Distributed Processing, Volume 1*. Cambridge, Mass.: MIT Press.

[117] Segev, I., Fleshman, J., and Burke, R. (1989). Compartmental models of complex neurons. In Koch, C. and Segev, I., editors, *Methods in Neuronal Modeling*. Cambridge, Mass.: MIT Press.

[118] Shao, Z. and Burkhalter, A. (1999). Role of GABA-B receptor-mediated inhibition in reciprocal inter-areal pathways of rat visual cortex. *J. Neurophysiol.*, 81:1014–24.

[119] Snodderly, D. M. and Gur, M. (1995). Organization of striate cortex of alert, trained monkeys (macaca fascicularis): Ongoing activity, stimulus selectivity, and widths of receptive field activating regions. *J. Neurophysiol.*, 64:2100–25.

[120] Somers, D. C., Todorov, E. V., Athanassios, G. S., Toth, L. J., Kim, D. S., and Sur, M. (1998). A local circuit approach to understanding integration of long-range inputs in primary visual cortex. *Cerebral Cortex*, 8:204–17.

[121] Somogyi, P. and Cowey, A. (1984). Double bouquet cells. In Jones, E. G. and Peters, A., editors, *Cerebral Cortex, Volume I: Cellular Components of the Cerebral Cortex*. New York: Plenum.

[122] Somogyi, P., Freund, T. F., and Cowey, A. (1982). The axo-axonic interneuron in the cerebral cortex of the rat, cat, and monkey. *Neurosci.*, 7:2577–07.

[123] Stratford, K. J., Tarczy-Hornoch, K., Martin, K. A., Bannister, N. J., and Jack, J. J. (1996). Excitatory synpatic inputs to spiny stellate cells in cat visual cortex. *Nature*, 382:258–61.

[124] Takeuchi, A. and Amari, S. (1979). Formation of topographic maps and columnar microstructures in nerve fields. *Biol. Cybern.*, 35:63–72.

[125] Tamas, G., Buhl, E., and Somogyi, P. (1997). Fast IPSPs elicited via multiple synaptic release sites by different types of gabaergic neurone in the cat visual cortex. *J. Physiol.*, 500:715–38.

[126] Tanaka, K. (1996). Inferotemporal cortex and object vision. *Ann. Rev. Neurosci.*, 19:109–39.

[127] Tanifuji, M., Sugiyama, T., and Murase, K. (1994). Horizontal propagation of excitation in rat visual cortical slices revealed by optical imaging. *Science*, 266:1057–9.

[128] Tanifuji, M., Yamanaka, A., Sunaba, R., Terakawa, S., and Toyama, K. (1996). Optical responses evoked by white matter stimulation in rat visual cortical slices and their relation to neural activities. *Brain Research*, 738:83–95.

[129] Tombol, T. (1984). Layer VI cells. In Jones, E. G. and Peters, A., editors, *Cerebral Cortex, Volume I: Cellular Components of the Cerebral Cortex*. New York: Plenum.

[130] Tsau, Y., Guan, L., and Wu, J. Y. (1998). Initiation of spontaneous epileptiform activity in the neocortical slice. *J. Neurophysiol.*, 80:978–82.

[131] van Laarhoven, P. J. M. and Aarts, E. H. L. (1987). *Simulated Annealing: Theory and Applications*. Dordrecht: D. Reidel.

[132] Vergnes, M., Boehrer, A., Simler, S., Bernasconi, R., and Marescaux, C. (1997). Opposite effects of GABAB receptor antagonists on absences and convulsive seizures. *Eur. J. Pharm.*, 332:245–55.

[133] Vogt, B. A. (1991). The role of layer I in cortical function. In Peters, A. and Jones, E. G., editors, *Cerebral Cortex, Volume IX: Normal and Altered States of Function*. New York: Plenum.

[134] White, E. L. (1989). *Cortical Circuits*. Boston: Birkhauser.

[135] Wilson, H. R. and Cowan, J. D. (1973). A mathematical theory of the functional dynamics of cortical and thalamic nervous tissue. *Kybernetik*, 13:35–80.

[136] Wilson, M. A. and Bower, J. M. (1989). The simulation of large-scale neural networks. In Koch, C. and Segev, I., editors, *Methods in Neuronal Modeling*. Cambridge, Mass.: MIT Press.

[137] Wiser, A. K. and Callaway, E. M. (1996). Contributions of individual layer 6 pyramidal neurons to local circuitry in macaque primary visual cortex. *J. Neurosci.*, 16:2724–39.

[138] Wiskott, L. and Sejnowski, T. (1998). Constrained optimization for neural map formation: A unifying framework for weight growth and normalization. *Neural Computation*, 10:671–716.

[139] Wörgötter, F. and Koch, C. (1991). A detailed model of the primary visual pathway in the cat: Comparison of afferent excitation and intracortical inhibitory connection schemes for orientation selectivity. *J. Neurosci.*, 11:1959–79.

[140] Young, M. P. (1993). The organization of neural systems in the primate cerebral cortex. *Proc. R. Soc. Lond. B*, 252:13–8.

[141] Zhang, K. (1996). Representation of spatial orientation by the intrinsic dynamics of the head-direction cell ensemble: A theory. *J. Neurosci.*, 16:2112–26.

[142] Zhang, Z. W. and Deschenes, M. (1997). Intracortical axonal projections of lamina VI cells of the primary somatosensory cortex in the rat: A single-cell labeling study. *J. Neurosci.*, 17:6365–6379.

[143] Zhou, F. M. and Hablitz, J. J. (1996). Morphological properties of intracellularly labeled layer I neurons in rat neocortex. *J. Comp. Neurol.*, 376:198–213.

[144] Zilles, K. J. (1985). *The Cortex of the Rat: A Stereotaxic Atlas*. Berlin: Springer-Verlag.

Figure Captions

Figure 1: Plot of typical pyramidal cell influence via axonal arbor on same compartment (left) and both other compartments combined (right); to scale, arbitrary units. The shape of the within-compartment influence results from superposition of 3 ranges of arbor width with different frequencies of occurrence – typically 0.5, 1, and 2 millimeters in the rat.

Figure 2: The left side illustrates the overall structure of both models: a stack of 2-dimensional lattices of cell populations at different densities; local radial connections exist both within and between lattices. The right side displays the laminar structure of the 6-layer architecture and the two simplified models, together with the numbers of excitatory and inhibitory (E/I) populations (each on its own lattice) in each layer.

Figure 3: Cell populations in the 6-layer architecture and the two simplified models, illustrating method of reduction by arbor averaging and consolidation. The drawings, all to the same scale, depict the widths and relative densities of arbors for layer III cells in the 6-layer architecture (top), for cells in all layers in the 3-layer model (middle), and for both cell populations in the 1-layer model (bottom). **Pyramidal cells** have their dendritic arbors drawn in black and their axonal arbors, always extending further out, shaded in each destination layer according to the percentage of the output sent there (higher = darker). The staggered shading in the 1-layer excitatory arbor indicates the result of combining influences from wide and narrow arbors (cf. the layer III pyramidal subtypes shown for the 6-layer architecture). Similar staggered weightings were employed in the 3-layer model but are not illustrated here for reasons of clarity. **Inhibitory cells** have their dendritic arbors in black and the axonal arbors (which always overlap the dendrites) outlined. (Types appear in order from left to right as listed in Tables 5,7). Notice the significant size difference between pyramidal and inhibitory arbors. The **consolidated inhibitories** sections illustrate the net output of all the inhibitory types with their cell bodies in a particular source layer – the width in a destination layer corresponds to the *widest* axonal arbor from any of the types while the percentage (illustrated by shading) is the average of that for all the types weighted by their relative population sizes.

Figure 4: Different patterns of pyramidal cell horizontal axonal arborization explored in the 1-layer model, to scale. Each plot represents the normalized, weighted sum of axonal arbors of all pyramidal subtypes at a range of horizontal distances (out to 1.5 millimeter radius) from a source position.

Figure 5: Model cell responses to current injection (1.0 nA) for 100 msec: top traces represent spiking, bottom membrane potential. **A:** Regular spiking pyramidal. **B:** Intrinsic burst pyramidal. **C:** Fast spiking inhibitory (0.5 nA injection).

Figure 6: Schematic of experimental setup employed by both Chagnac-Amitai & Connors and Langdon & Sur; see text for details.

Figure 7: Modes of response of 1-layer model to current injection at a single point. From left to right, quiescence regime, explosion regime, wave propagation regime. *Upper plots* display membrane potential traces of single pyramidal cells spaced at 600 μm intervals along a line starting at the stimulation point, for 100 msec (left, right) or 50 msec (middle) immediately following stimulation. *Lower plots* are snapshots of the excitatory cell instantaneous firing rates,

averaged over 4x4 cells spatially, at 8 msec (quiescence) and 16 msec (explosion and wave regimes) post-stimulation – lighter shade indicates higher activity. (Activity had died in the quiescence case by 16 msec, while the wave and explosion regimes looked similar to each other at 8 msec.) Plots are rectangular because a 2x4 mm sheet was simulated.

Figure 8: Propagation speeds (in μm/msec) for a range of parameter values in wave regime. **A:** Plotted for several inhibition levels (expressed as a ratio to the baseline, balanced level), for each of the pyramidal arborization patterns investigated. For each pattern, seven evenly spaced inhibition levels are plotted; the lowest and highest one or two of these fall in the explosion and quiesecence regimes respectively, while the others are in the wave regime. The curves have been aligned relative to one another on the basis of response level because of differing excitabilities for the different connectivity patterns (see text). **B:** Plotted for a range of excitatory-excitatory synaptic strengths (as shown, in nanoSiemens) for the Short connectivity. Each data point is the average of 4 runs with different inhibition levels, within the wave regime if possible (it was not for the lowest and highest levels shown which gave only explosion and quiescence respectively). **C:** Plotted for a range of inhibitory-excitatory connection lengths while all other lengths are as in the Short condition; lengths shown include dendritic distance. **D:** Plotted for a range of excitatory-excitatory lengths, holding the falloff constant at $\lambda = 625\mu$m.

Figure 9: Differences in monosynaptic transmission distance. Each of the three plots displays membrane potential for model cells at successively further points from the origin (top trace), as in Figure 7, top. The vertical lines indicate the first peaks of the traces; in each case, there is a jump from peaks being within < 5 msec (a shorter time than required for charging and synaptic transmission) of each other to being much further apart. For the Baseline case, this occurs between 300 and 600 μm, for the average and fit cases, between 600 and 1200 μm.

Figure 10: Activity in superficial, middle, and deep (infragranular) layers in 3-layer model during wave propagation. Left side shows membrane potential traces as in Figure 7, top for 4 locations over 30 msec. The plots on the right display spiking activity of all the pyramidal cells in each layer for three successive times: 0, 12, and 24 msec: each point is the firing rate averaged locally over 4x4 cells and 2 msec. Different square sizes reflect differing numbers of pyramidal cells in the three layers.

Figure 11: Average instantaneous firing rates over entire layer (averaged over 4x4 cells spatially) for superficial (dotted traces), middle (dashed), and deep (solid) pyramidal cells in three versions of the model: baseline, evenly-connected, and no between-layer inhibition. Note that the laminar activity difference is small and inconsistent in the second version, and small in the third. (Traces are from typical runs within the wave regime.)

Figure 12: Activity plots for pyramidal (large, upper rectangular grids) and small inhibitory (small, lower grids) cells in each layer for the evenly-connected simulation in Figure 11. Graphical format as in Figure 10. Excitatory activities fluctuate, but remain essentially equal in magnitude across the 3 layers. Inhibitory activities follow the excitatory but sometimes lag behind. Asymmetry in wave propagation, typical near the quiescence regime, occurred as a result of threshold variability in the model cells.

Figure 13: Cortical interaction functions. **A:** The top superimposes the widest interaction function employed by Miller (1994) with our 'Short' horizontal pyramidal arbor, while the bottom illustrates our 'Baseline' arbor (all three normalized to same area). **B:** The corresponding arbors for interactions within and between layers in our 3-layer model

are shown in matrix form (includes effects of inhibitory interactions; see text). Width of x-axis in all plots is 3 mm.

Table Captions

Table 1: Proportions of excitatory and inhibitory cell populations in each layer in rat koniocortical areas 17 and Par1. *Note 1:* Because there is no sharp change in pyramidal soma size and packing density between layers II and III in these areas, Beaulieu did not distinguish them. Nevertheless, layer II pyramidal cells are known to have different morphology from layer III pyramidal cells (see text), therefore we imposed an arbitrary but reasonable division by assigning 1/3 of the counted cells for the combined II/III to layer II, and 2/3 to layer III.

Table 2: Dendrite and axon arbors for pyramidal cells in rat koniocortex. Each arbor is given in terms of the percentage and diameter (in μm) ramifying in each layer. For each dendritic type in the second column, one or more correlated axonal types are given in the third (axon arbors are more various).

Table 3: Synaptic input to pyramidal cells. After DeFelipe & Farinas (1992).

Table 4: Classes of inhibitory cells in model. All outputs are to pyramidal cells unless noted, determined from electron microscope studies; percentages in parentheses are estimated. (B)=GABA$_B$; spider-web cells also called neurogliaform by some authors. The letters next to the references indicate (species: lobe cortical type): (Rat/Cat/Monkey: Occipital/Temporal/Parietal/Frontal Konio-/Iso-/Agranular cortex). '*' indicates results were reported for multiple species/area combinations.

Table 5: Arborization characteristics of inhibitory cells in layer III. Each row gives the percentages and radii of axon and dendrite arbors (in μm) in each layer for a given cell subpopulation in layer III. The full table is available through `http://zakros.ucsd.edu/~arobert/CorticalData/`.

Table 6: List of densities and interconnections for layer III in the 6-layer architecture specification (the full table is available from `http://zakros.ucsd.edu/~arobert/CorticalData/`). Each matrix entry represents the number of input synapses supplied by cells of the source population to each cell of the target population. To obtain the number of connections *output* by each cell in the source population, multiply by the ratio of target to source density. In cases where the same population supplies input of more than one type to another (Basket cells supply somatic, dendritic, and spine inhibition to pyramidal cells, spiderweb and arcade cells supply somatic and dendritic inhibition, and bipolar cells supply GABA$_A$ and GABA$_B$ inhibition), the multiple entries are separated by commas.

Table 7: Full list of arborizations in 3-layer model, in the same format as Table 5 for the 6-layer specification.

Table 8: Full list of population sizes and interconnections in 3-layer model, in the same format as Table 6 for the 6-layer specification. All entries represent scaled values, as described in text. Both small and wide cells act like basket, spider-web, and arcade cells in the 6-layer architecture in supplying somatic and dendritic inhibition. Here, totals are also given for outputs from each cell (right-hand column) and total inputs to each cell (bottom row, I$_A$ and I$_B$ stand for GABA$_A$ and GABA$_B$ inhibition). Note the percentages for E and I differ from the anatomical values because the inhibitory cell populations were not reduced as much as the pyramidal cell populations were (see Methods).

Table 9: Parameter dependence in the single layer model. I-E stands for inhibitory-excitatory connections and so

on; d_c is the highest inhibition level at which the network displayed the explosion regime, expressed as the ratio of the strength of $GABA_A$ synapses at the transition to that at baseline. Ranges of variation are given as ratios to the baseline value in the form [min,max].

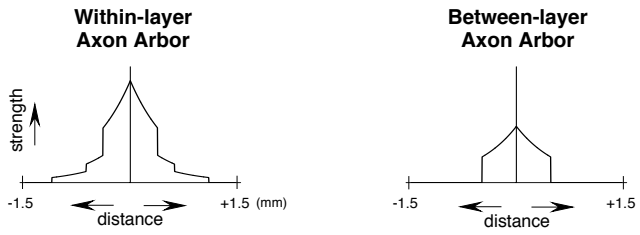
Within-layer
Axon Arbor
strength
-1.5
distance
+1.5 (mm)
Between-layer
Axon Arbor
-1.5
distance
+1.5

Figure 1:

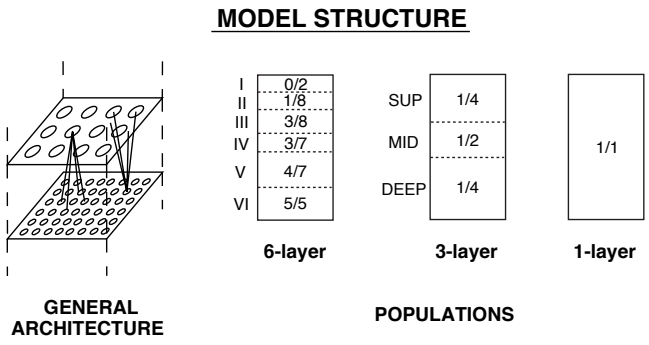
MODEL STRUCTURE
I
II
III
IV
V
VI
0/2
1/8
3/8
3/7
4/7
5/5
SUP
MID
DEEP
1/4
1/2
1/4
1/1
6-layer
3-layer
1-layer
GENERAL ARCHITECTURE
POPULATIONS

Figure 2:

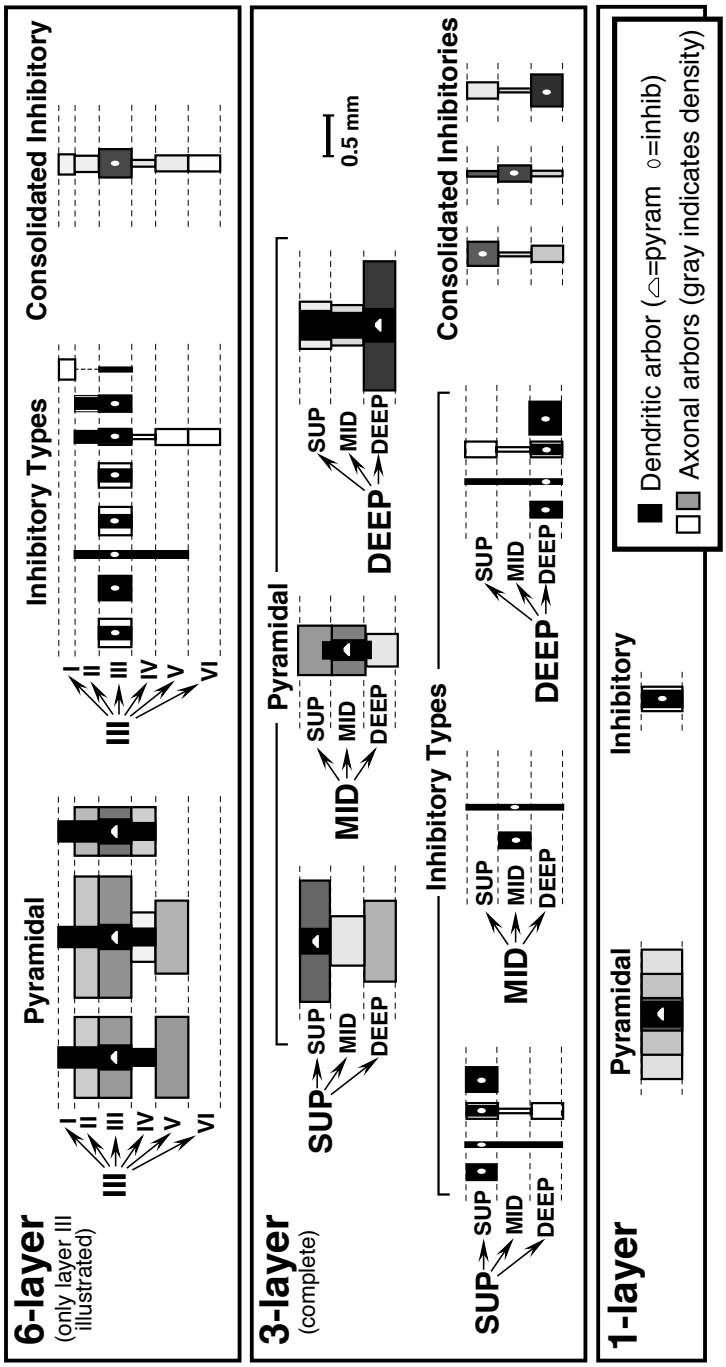
6-layer
(only layer III illustrated)
Pyramidal
Inhibitory Types
Consolidated Inhibitory
I
II
III
IV
V
VI
3-layer
(complete)
SUP
MID
DEEP
0.5 mm
Inhibitory Types
Consolidated Inhibitories
1-layer
Pyramidal
Inhibitory
Dendritic arbor (△=pyram ○=inhib)
Axonal arbors (gray indicates density)

Figure 3:

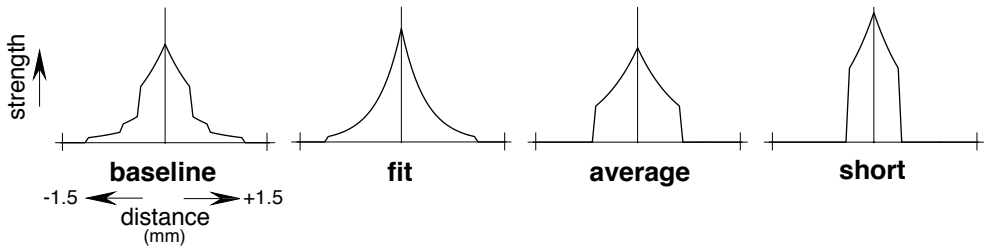

Figure 4:

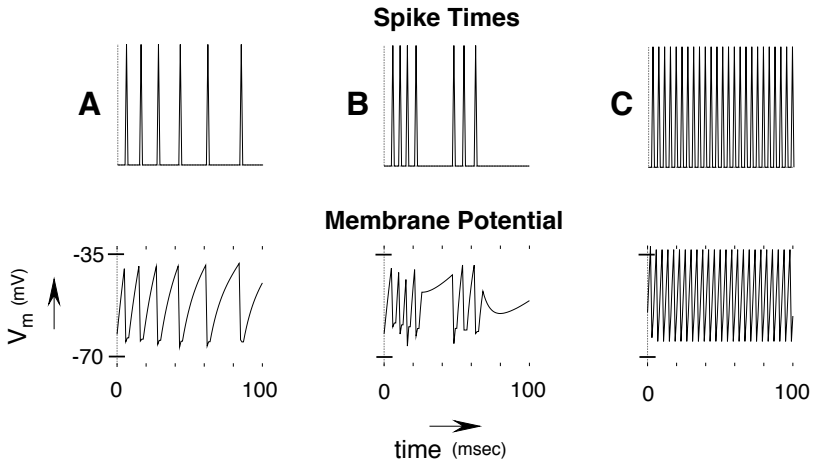
Spike Times
A
B
C
Membrane Potential
-35
-70
V_m (mV)
0
100
0
100
0
100
time (msec)

Figure 5:

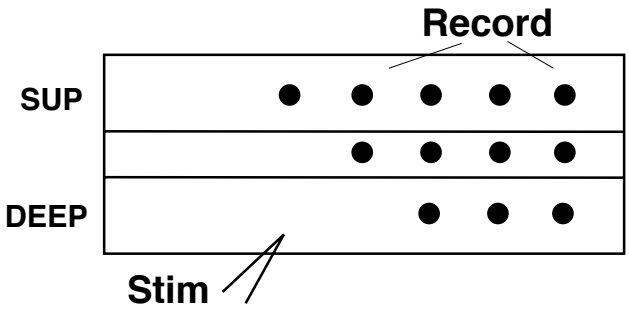

Figure 6:

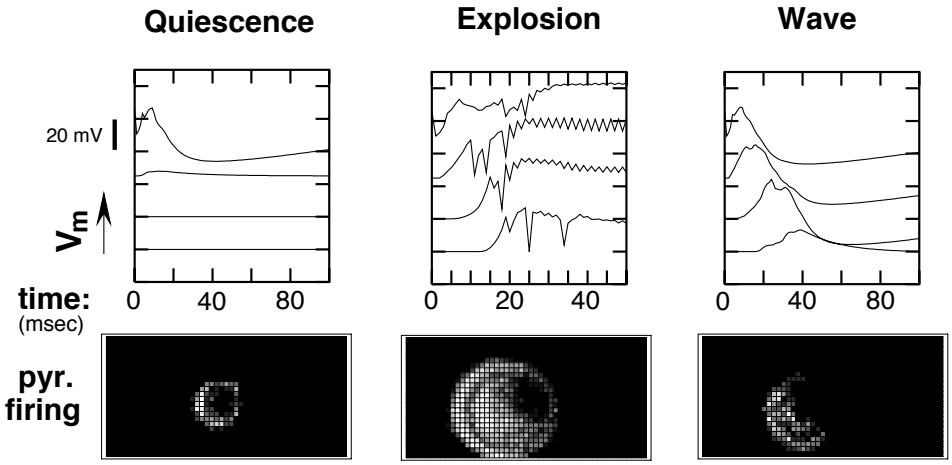
Quiescence
Explosion
Wave
20 mV
V_m
time:
(msec)
0
40
80
0
20
40
0
40
80
pyr.
firing

Figure 7:

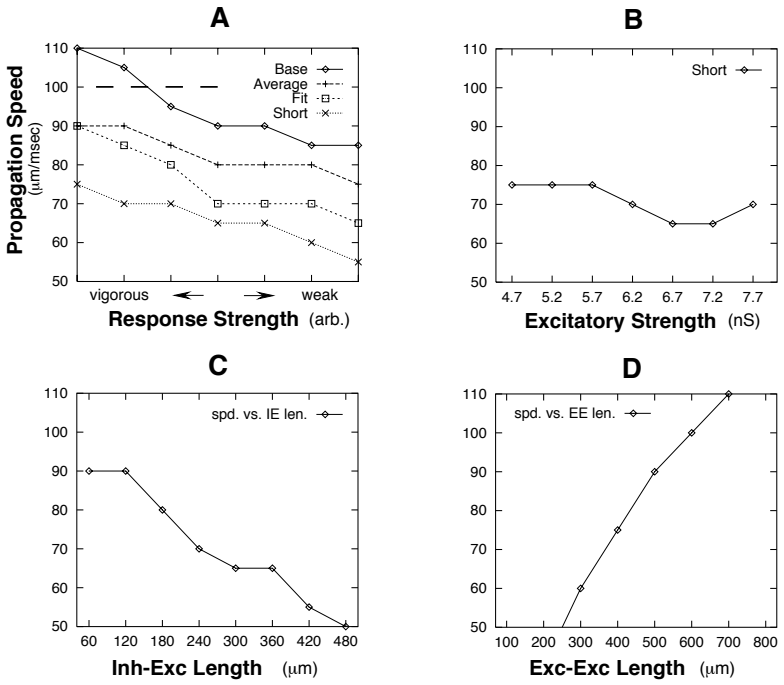
A
B
C
D
Propagation Speed
(μm/msec)
Base
Average
Fit
Short
vigorous
weak
Response Strength (arb.)
Short
Excitatory Strength (nS)
spd. vs. IE len.
Inh-Exc Length (μm)
spd. vs. EE len.
Exc-Exc Length (μm)

Figure 8:

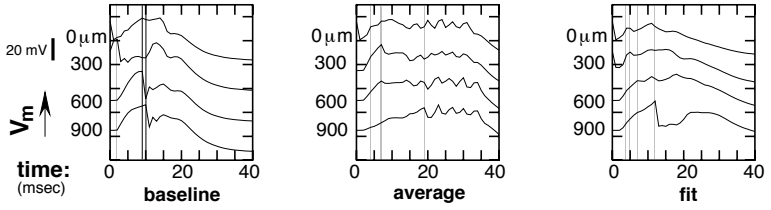

Figure 9:

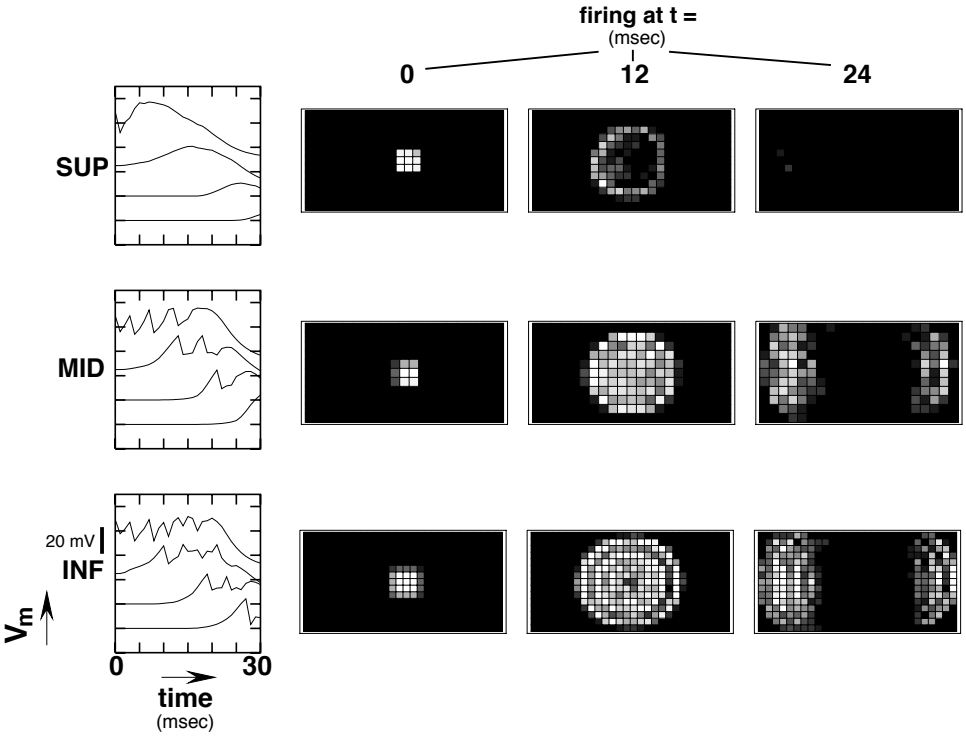

Figure 10:

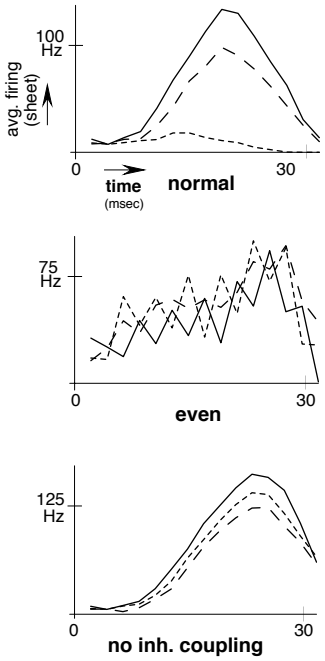
100
Hz
avg. firing
(sheet)
0
30
time
(msec)
normal
75
Hz
0
30
even
125
Hz
0
30
no inh. coupling

Figure 11:

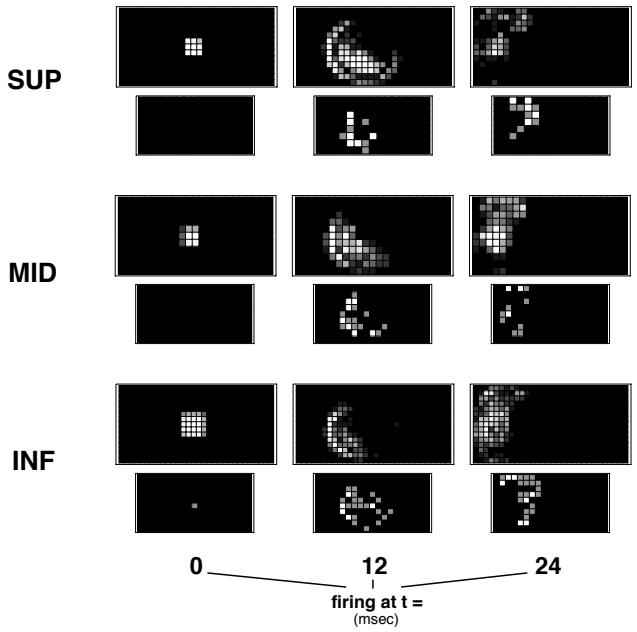

Figure 12:

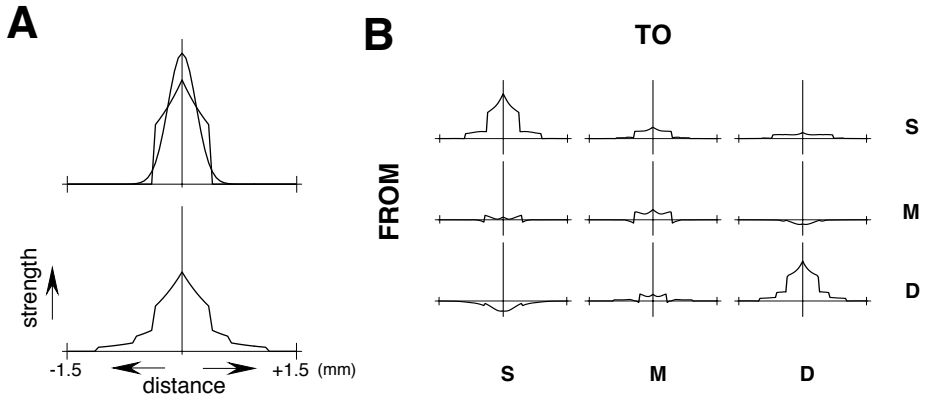

Figure 13:

Distribution of Excitatory and Inhibitory Cells Across Cortical Layers

Layer	Exc Pop (%)	Inh Pop (%)	Subpopulations
I	0	4	Cajal-Retzius, small neuron of layer I
II[1]	10	10	pyramidal (1), chandelier, basket, bipolar, spider-web, arcade, ascending/descending, superficial plexus, Martinotti
III	20	19	pyramidal (3), chandelier, basket, bipolar, spider-web, arcade, ascending/descending, superficial plexus, Martinotti
IV	22	15	pyramidal (1), spiny stellate (2), chandelier, basket, bipolar spider-web, arcade, superficial plexus, Martinotti
V	18	27	pyramidal (4), chandelier, basket, bipolar spider-web, arcade, ascending/descending, Martinotti
VI	30	25	pyramidal (5), basket, spider-web, arcade, ascending/descending, ovoid

Table 1:

Pyramidal Cell Dendrite and Axon Distribution

Layer	Dendritic Arbor Types	Axonal Arbor Types
II	33% 280 in I, 61% 280 in II, 6% 280 in III	25% 600 in II/III, 15% 1200 in II/III, 10% 600 in IV, 35% 900 in V, 10% 2400 in V, 5% 1000 in VI
III	7% 200 in I, 23% 200 in II, 67% 300 in III, 3% 200 in IV	60% 1000 in II/III, 40% 1000 in V 65% 1500 in II/III, 5% 600 in IV, 30% 900 in V 80% 600 in II/III, 20% 600 in IV
IV	10% 100 in II/III, 90% 200 in IV	46% 400 in II/III, 27% 300 in IV, 17% 400 in V, 10% 400 in VI
V	1% 50 in II, 2% 50 in III, 7% 100 in IV, 85% 300 in V, 5% 200 in VI 10% 250 in I, 6% 50 in II, 7% 100 in III, 9% 300 in IV, 68% 350 in V	10% 700 in III, 25% 600 in IV, 45% 600 in V, 20% 800 in VI 5% 300 in III, 10% 100 in IV, 55% 1400 in V, 30% 1800 in VI 15% 600 in III, 25% 600 in IV, 55% 1200 in V, 5% 100 in VI
VI	10% 100 in IV, 15% 150 in V, 75% 200 in VI 20% 200 in V, 80% 250 in VI 10% 100 in IV, 15% 300 in V, 75% 400 in VI 100% 300 in VI 100% 500 in VI	11% 200 in III, 32% 300 in IV, 32% 300 in V, 25% 300 in VI 5% 100 in IV, 55% 600 in V, 40% 500 in VI 13% 500 in V, 87% 2200 in VI 5% 500 in III, 5% 500 in IV, 50% 2000 in V, 40% 2000 in VI 15% 1200 in III, 25% 1200 in IV, 20% 1100 in V, 40% 1000 in VI

Table 2:

Anatomical Synapses onto Pyramidal Cells

Portion	Number	Notes
Axon init. seg. (inh)	2/19/25	numbers for corticothalamic, callosal, and ipsilateral projection cells in cat respectively
soma	70/270	numbers for corticothalamic, callosal projection cells in cat, respectively
spine (exc)	8000	
spine (inh)	300	differing estimates in literature
shaft (exc)	600	
shaft (inh)	1100	differing estimates in literature

Table 3:

Inhibitory Types: Observed Outputs and References

Celltype	Layers	Outputs	References
chandelier	II-V	100% axon-initial segment	DeFelipe et al., 1985 (M:FA); DeFelipe et al., 1989 (M); Del Rio & DeFelipe, 1994 (H:T); Fonseca et al., 1993 (H:T); Lewis & Lund, 1990 (M:FI); Marin-Padilla, 1987 (H:OK); Peters, 1984 (*); Somogyi et al., 1982 (RCM:OK/I)
basket	II-VI	30% soma, 20% spine, 40% shaft, 10% inh shaft or soma	DeFelipe et al., 1986 (M:FA); Jones & Hendry, 1984 (*); Kisvarday & Eysel, 1990 (H:*I); Kisvarday & Eysel, 1993 (C:OK); Kisvarday et al., 1993 (C:OI); Martin et al., 1983 (C:OK); Peters & Harriman, 1992 (R:OK)
bipolar	II-V	40% spine (B), 40% shaft (B), 20% inh shaft	de Lima & Morrison, 1989 (M:OK/I,T*); Gabbott & Bacon, 1996 (M:F*); Gabbott et al., 1997 (R:F*); Gonchar & Burkhalter, 1999 (R:OK); Jones et al., 1987 (M:*); Peters & Harriman, 1988 (R:OK); Peters, 1984 (*)
spider-web	II-VI	(40%) soma, (60%) shaft	Gabbott et al., 1997 (R:F*); Jones, 1984 (*); Kisvarday et al., 1990 (H:*I); Lund & Lewis, 1993 (M:FI)
arcade	II-VI	(40%) soma, (60%) shaft	Lund & Lewis, 1993 (M:FI); Peters & Saint Marie, 1984 (*)
ascending/descending	II-II, V-VI	100% shaft	Lund & Lewis, 1993 (M:FI); Peters & Saint Marie, 1984 (*)
superficial plexus	II-IV	100% shaft	Lund & Lewis, 1993 (M:FI); Peters & Saint Marie, 1984 (*)
Cajal-Retzius	I	100% apical tuft shaft (B)	Marin-Padilla, 1984 (*), 1990 (H:*); Zhou & Hablitz, 1996 (R:*)
Martinotti	II-V	100% apical tuft shaft	Braitenberg, 1991 (R:*); Marin-Padilla, 1990 (H:*); Peters & Saint Marie, 1984 (*); Zhou & Hablitz, 1996 (R:*)
small neuron of layer I	I	48% apical tuft spine (B), 48% apical tuft shaft (B), 4% inhibitory soma	Marin-Padilla, 1984 (*), 1990 (H:*); Martin et al., 1989 (C:OK); Zhou & Hablitz, 1996 (R:*)
ovoid neuron of layer VI	VI	100% shaft	Tombol, 1984 (*)

Table 4:

Summarized Data on Layer III Cell Arbors

Type	AXONAL ARBOR												DENDRITIC ARBOR											
	Percentage						Radius (μm)						Percentage						Radius (μm)					
	I	II	III	IV	V	VI	I	II	III	IV	V	VI	I	II	III	IV	V	VI	I	II	III	IV	V	VI
Chandelier	0	0	100	0	0	0	0	0	175	0	0	0	0	0	100	0	0	0	0	0	75	0	0	0
Basket	0	0	100	0	0	0	0	0	150	0	0	0	0	0	100	0	0	0	0	0	150	0	0	0
Bipolar	0	5	50	25	20	0	0	40	40	40	40	0	10	20	50	10	10	0	0	40	40	40	40	0
Spider-web	0	0	100	0	0	0	0	0	175	0	0	0	0	0	100	0	0	0	0	0	75	0	0	0
Arcade	0	0	100	0	0	0	0	0	150	0	0	0	0	0	100	0	0	0	0	0	75	0	0	0
Asc./Desc.	0	0	40	10	25	25	0	0	75	30	100	100	0	20	80	0	0	0	0	75	100	0	0	0
Sup. Plexus	0	20	80	0	0	0	0	100	100	0	0	0	0	20	80	0	0	0	0	75	100	0	0	0
Martinotti	100	0	0	0	0	0	120	0	0	0	0	0	0	0	100	0	0	0	0	0	30	0	0	0

Table 5:

Optimized Connectivity Matrix, Layer III of 6-Layer Architecture

		Number of Synapses In to Type										
Density	**Type**	Pyramidal	Pyramidal	Pyramidal	Chandelier	Basket	Bipolar	Spider-web	Arcade	Asc./Desc.	Sup. Plexus	Martinotti
4920	Pyramidal	605	605	605	80	80	79	80	80	92	92	80
4920	Pyramidal	656	656	656	86	86	85	86	86	99	99	86
4920	Pyramidal	827	827	827	108	108	100	108	108	123	123	108
117	Chandelier	12	12	12	0	0	0	0	0	0	0	0
373	Basket	70,210	70,210	70,210	0	155	0	0	0	0	0	0
794	Bipolar	93,82	93,82	93,82	86	0	72	86	86	80	80	86
273	Spider-web	73,118	73,118	73,118	0	0	0	0	0	0	0	0
290	Arcade	76,122	76,122	76,122	0	0	0	0	0	0	0	0
118	Asc./Desc.	63	63	63	0	0	0	0	0	0	0	0
498	Sup. Plexus	170	170	170	0	0	0	0	0	0	0	0
107	Martinotti	13	13	13	0	0	0	0	0	0	0	0

Table 6:

Cell Arbors in 3-Layer Model

Layer	Type	AXON						DENDRITE					
		Percentage			Radius (μm)			Percentage			Radius (μm)		
		sup	mid	deep	sup	mid	deep	sup	mid	deep	sup	mid	deep
Sup	**pyramidal**	60	10	30	750	300	500	100	0	0	150	0	0
	small	100	0	0	100	0	0	100	0	0	100	0	0
	wide	100	0	0	150	0	0	100	0	0	150	0	0
	bipolar	40	20	40	40	40	40	60	30	10	40	40	40
	asc./desc.	30	30	40	100	40	100	100	0	0	80	0	0
Mid	**sp. stell.**	40	50	10	300	300	200	10	80	10	100	120	100
	small	0	100	0	0	100	0	0	100	0	0	100	0
	bipolar	30	20	50	40	40	40	30	40	30	40	40	40
Deep	**pyramidal**	7	15	78	300	200	800	10	8	82	180	150	200
	small	0	0	100	0	0	100	0	0	100	0	0	100
	wide	0	0	100	0	0	200	0	0	100	0	0	150
	bipolar	25	25	50	40	40	40	30	30	40	40	40	40
	asc./desc.	30	17	53	100	40	100	0	0	100	0	0	80

Table 7:

Optimized Connectivity Matrix, 3-Layer Model

		Number of Synapses In to Type													
Density	**Type**	Pyramidal	Small	Wide	Bipolar	Asc./Desc.	Sp. Stellate	Small	Bipolar	Pyramidal	Small	Wide	Bipolar	Asc./Desc.	Total Out (E/I)
720	Pyramidal	90	20	20	13	20	31	5	9	28	6	6	9	6	149/114
60	Small	3,9	0	0	0	0	0	0	0	0	0	0	0	0	12/0
59	Wide	3,9	0	8	0	0	0	0	0	0	0	0	0	0	12/8
62	Bipolar	2,2	3	0	3	3	1,1	2	2	1,1	2	0	2	2	8/19
72	Asc./Desc.	4	0	0	0	0	5	0	0	3	0	0	0	0	12/0
528	Sp. Stellate	22	10	10	11	10	36	17	10	6	1	1	9	1	64/80
89	Small	0	0	0	0	0	6,18	0	0	0	0	0	0	0	24/0
42	Bipolar	1,1	2	0	1	2	0,0	1	1	1,1	2	0	0	2	4/11
1152	Pyramidal	17	4	4	9	4	32	11	13	93	25	25	14	25	142/134
95	Small	0	0	0	0	0	0	0	0	3,9	0	0	0	0	12/0
94	Wide	0	0	0	0	0	0	0	0	3,9	0	8	0	0	12/8
97	Bipolar	2,2	3	0	3	3	3,3	4	3	3,3	4	0	3	4	16/27
132	Asc./Desc.	8	0	0	0	0	5	0	0	7	0	0	0	0	20/0
2400/802	Total In ($E/I_A/I_B$)	129/43/5	34/8	34/8	33/7	34/8	99/38/4	33/7	32/6	127/42/5	32/8	32/8	32/5	32/8	

Table 8:

Functional Effects of Parameter Variations, 1-Layer Model

Parameter	Range	Effects	Explanation for Effects
I-E length	[0.5,2.0]	this parameter affected the wave thickness and speed but not d_c: the greater the length, the wider and slower the waves	wider radius dilutes inhibitory effect but increases excitatory charging times at longer distances
I-I length	[0.5,4.0]	both decreasing and increasing this length led to a narrower transition between the quiescence and explosion regimes (i.e., a narrower wave regime); d_c was not affected	unclear
$GABA_B$ length	[0.5,4.0]	shorter lengths gave narrower wave regimes	the quashing influence of $GABA_B$ is responsible for restricting explosions to waves; when it is more radially localized, it is easier for excitation to outrace it
E-E strength	[0.7,1.2]	increasing overall E-E strength raised d_c	cells receive greater excitatory drive while increase in inhibitory regulation comes only at a time delay
$GABA_B$ strength	[0.0,2.0]	greater strength gave more tightly organized wave progression and an increase in d_c, while weaker strength gave messier and generally thicker waves and a lower d_c	the delayed quashing of activity by $GABA_B$ is largely responsible for the form of the waves

Table 9: